Theory of coherent optical transients with quantized atomic motion

P. R. Berman, H. Nguyen, and A. Kuzmich
Department of Physics, University of Michigan, Ann Arbor, Michigan 48109, USA

(Received 9 November 2018; published 22 January 2019)

A theory of coherent transients is developed in which a sequence of optical pulses is incident on a sample of trapped atoms and gives rise to phase-matched emission from the sample. The trapping potential for the atoms can be state dependent, necessitating a quantum treatment of the center-of-mass motion. A source-field approach is followed, modified to account for the quantized motion of the atoms. The theory is illustrated with two examples, one involving the creation of ground-Rydberg level coherence in an optical lattice and the second Raman coherence between two ground-state sublevels of atoms in a dipole trap. For state-independent potentials, a comparison is made with a theory in which the center-of-mass motion is treated classically.

DOI: 10.1103/PhysRevA.99.013427

I. INTRODUCTION

Coherent transients provide an important probe of atomic and molecular systems. Historically, the field of coherent transients was developed within the context of nuclear magnetic resonance (NMR). In NMR a series of radio-frequency pulses is applied to a spin system [1]. In response to the applied pulses, the sample emits a coherent signal that can be used to measure spin relaxation rates. With the development of laser sources, the coherent transient technique was extended to the optical domain [2]. A series of optical pulses is applied to an atomic or molecular sample, resulting in phase-matched, coherent emission from the sample. Such coherent optical transients (COT) can be used to measure the relaxation rates of the various atomic coherences that are produced by the incident pulses. In both NMR and COT, inhomogeneous variations in the transition frequencies of the spins or atoms can result in significant damping of the generated signals. In NMR, stray magnetic fields modify the separation between spin magnetic sublevels while in COT the Doppler shift associated with atomic motion leads to the inhomogeneities. Spin echoes and photon echoes represent coherent transient techniques that can be used to suppress the effects of magnetic field or Doppler dephasing.

A somewhat more direct way of eliminating Doppler dephasing is to cool atoms. However, even at temperatures of tens of microkelvins that can be achieved using standard laser cooling techniques, Doppler dephasing can still be the dominant factor that limits the lifetimes of long-lived atomic coherences. To further reduce any effects of motional or Doppler dephasing, atoms can be trapped in optical potentials that confine the atoms to distances that are much smaller than the relevant optical wavelengths [3]. This is akin to Dicke narrowing [4], where collisions of atoms with a background buffer gas effectively restrict the atoms to a small volume for the duration of a given experiment. To observe Dicke narrowing, there is a subtle effect that enters. If the collision interaction between the buffer gas and the atoms is state dependent, that is, if the collision interaction differs for the two atomic states of an optical transition, then the mechanism responsible for Dicke narrowing can be totally suppressed [5]. In such cases, the atomic center-of-mass motion must be quantized to properly model the system. The same can be said for trapping by optical potentials. If phase-matched emission results from coherence between two atomic levels for which the optical potentials are different, the atomic motion in the trapping potentials must be treated using a fully quantum theory.

Light-matter interfaces and quantum memories based on Raman scattering [6,7] or excitation to Rydberg levels [8,9] in atomic ensembles are well-known applications of COT. Such systems have been studied intensely in the past two decades. Much of the experimental and theoretical work in this area was focused on situations in which atoms are not subjected to external forces. On the other hand, there are experiments aimed at achieving long-term ($\geqslant$1 s) quantum state storage that make use of atomic confinement, typically employing far-detuned optical fields [10–12]. The atomic state dynamics is then governed by the periodic motion in the confining potentials, with a corresponding modulation of the strength of atom-light coupling and memory storage and retrieval efficiencies.

Although there have been numerous papers written related to the interaction of optical fields with trapped atoms in the context of laser cooling [13], light scattering [14], fluorescence [15], and wave-packet oscillations [16], there have been only a few articles that addressed phase-matched emission from trapped atoms. Zhao *et al.* [17] and Jenkins *et al.* [18] calculated the phase-matched emission from an ensemble of trapped atoms following a Raman excitation pulse and a readout pulse. Recently, Lampen *et al.* [19] presented both theoretical and experimental results for phase-matched emission from an ensemble of trapped atoms using pulsed, two-photon excitation of a Rydberg level pulse followed by a readout pulse. There are also related calculations carried out within the context of atom interferometry [20]. However, to our knowledge, a general theory of optical coherent transients from trapped atoms based on a source-field approach [21] that includes the effects of quantized motion in state-dependent trapping potentials has not yet been developed.

 ©2019 American Physical Society

In this paper, we formulate a general theory of coherent transient spectroscopy that incorporates a quantum description of the atomic center-of-mass motion. In Sec. II, we calculate the change in atomic density matrix elements produced by an optical pulse acting on a generic two-level atomic system. The transfer matrix associated with such a process is the building-block solution from which the more general response of the atoms to a number of pulses can be calculated. In Sec. III, source-field theory [21], modified to include quantized center-of-mass motion for the atoms, is used to calculate the phase-matched coherent transient signal emitted by a sample of atoms. In Secs. IV and V, we present two examples to illustrate the theory. The first involves the creation and probing of ground-Rydberg level coherence in an optical lattice and the second the effect of transit-time loss on Raman coherence between ground-state sublevels. For state-dependent optical potentials, a quantized treatment of the center-of-mass motion is needed. However, under suitable initial conditions, a classical description of the center-of-mass motion can be used, provided the optical potentials are identical for the relevant atomic levels. In this limit, closed-form expressions for the radiated signal are obtained with and without the assumption of classical center-of-mass motion. The results are summarized in Sec. VI. The atomic density is assumed to be sufficiently low to neglect all atom-atom interactions.

II. PULSED EXCITATION: TRANSFER MATRIX

A. Excitation pulses

The atoms are subjected to a series of classical optical pulses. In this section, we calculate the response of a generic "two-level" atom (lower level a, upper level c, transition frequency ω_{ca}) to the nth pulse in this series. The incident fields are assumed to propagate in the X direction and be polarized in the z direction. In a paraxial wave approximation, the electric field of the nth pulse in the sample is given by

$$\mathbf{E}_n(\mathbf{R},t)=\tfrac{1}{2}\mathbf{u}_z E_n(t)f_n(\mathbf{R})e^{i(k_nX-\omega_nt)}+\text{c.c.}, \tag{1}$$

where $E_n(t)$ is the pulse amplitude at the center of the sample, $f_n(\mathbf{R})$ is the (real) spatial profile of the field in the sample, $\mathbf{u}_z$ is a unit vector in the z direction, $k_n=\omega_n/c$ is a propagation constant, and "c.c." stands for "complex conjugate." The pulse duration T_{p_n} is assumed to be sufficiently large to ensure that the spatial extent of the pulse is much larger than the sample length L. As a consequence, the pulse amplitude $E_n(t)$ reaches its maximum at approximately the same time for all atoms in the sample: this time is denoted by t_n. In other words, it is assumed that the spatial profile of the pulses can be taken to be constant during the atom-field interaction.

In addition to their interaction with the applied field pulses, the atoms are continuously subjected to optical trap fields that result in state-dependent optical potentials. The optical potentials associated with levels a and c are denoted by $V_a(\mathbf{R})$ and $V_c(\mathbf{R})$, respectively. For an atom having mass M, the eigenenergies of the Hamiltonian

$$H_\alpha(\mathbf{R})=-\frac{\hbar^2\nabla_R^2}{2M}+V_\alpha(\mathbf{R})\quad(\alpha=a,c) \tag{2}$$

are denoted by $\hbar\tilde{\omega}_{\alpha q}$, the eigenkets by $|\alpha q\rangle$, and the eigenfunctions by $\psi_{\alpha q}(\mathbf{R})$, where q represents the set of quantum numbers needed to label all the quantum numbers associated with the potential $V_\alpha(\mathbf{R})$. The eigenfunctions $\psi_{aq}(\mathbf{R})$ and $\psi_{cq'}(\mathbf{R})$ are *not* orthogonal for $q\neq q'$ if the potential is state dependent.

In the rotating-wave approximation (RWA), the Hamiltonian is taken as

$$H_n=\hbar\omega_a|a\rangle\langle a|+\hbar\omega_c|c\rangle\langle c|+\sum_q(\hbar\tilde{\omega}_{aq}|aq\rangle\langle aq|+\hbar\tilde{\omega}_{cq}|cq\rangle\langle cq|)+\frac{\hbar\Omega_{ca}^{(n)}(t)}{2}\sum_{j=1}^{N}f_n(\mathbf{R}_j)\begin{bmatrix}e^{ik_nX_j}e^{-i\omega_nt}\sigma_{ca}^{(j)}\\+e^{-ik_nX_j}e^{i\omega_nt}\sigma_{ac}^{(j)}\end{bmatrix}, \tag{3}$$

where $\Omega_{ca}^{(n)}(t)=-\mu_{ca}E_n(t)/\hbar$ (assumed real) is a Rabi frequency associated with the a-c transition, μ_{ca} is an electric dipole transition matrix element, $\sigma_{ca}^{(j)}$ ($\sigma_{ac}^{(j)}$) is a raising (lowering) operator for atom j, and N is the number of atoms. It is important to recognize that X_j is an *operator*: it is the X component of the position operator of atom j. The field is taken to be resonant with the atomic transition $\omega_n=\omega_{ca}$.

Our goal is to calculate the change in density matrix elements of atom j resulting from the applied pulse. In this section, we drop the j and n labels, but it is to be understood that all quantities refer to the time evolution of atom j during the nth pulse [for example, $f_n(\mathbf{R}_j)\to f(\mathbf{R})$, $\mathbf{k}_n\to\mathbf{k}$, etc.]; these labels will be restored in Sec. III. In the Schrödinger representation, density matrix elements obey the time-evolution equation

$$\dot{\rho}_{\alpha q;\alpha' q'}=\frac{1}{i\hbar}[H,\rho]_{\alpha q;\alpha' q'}. \tag{4}$$

Defining an interaction representation by

$$\rho_{\alpha q;\alpha' q'}=\rho^I_{\alpha q;\alpha' q'}\exp[-i\omega_{\alpha\alpha'}t-i\omega_{\alpha q,\alpha' q'}t], \tag{5}$$

where

$$\omega_{\alpha\alpha'}=\omega_\alpha-\omega_{\alpha'};\quad \omega_{\alpha q,\alpha' q'}=\tilde{\omega}_{\alpha q}-\tilde{\omega}_{\alpha' q'}, \tag{6}$$

we find time-evolution equations

$$\dot{\rho}^I_{aq;cp}=-i\frac{\Omega_{ca}(t)}{2}\begin{bmatrix}\sum_{p'}e^{i\omega_{aq,cp'}t}B^\dagger_{aq,cp'}(\mathbf{k})\rho^I_{cp';cp}\\-\sum_{q'}e^{i\omega_{aq',cp}t}\rho^I_{aq;aq'}B^\dagger_{aq',cp}(\mathbf{k})\end{bmatrix}, \tag{7a}$$

$$\dot{\rho}^I_{cp;aq}=-i\frac{\Omega_{ca}(t)}{2}\begin{bmatrix}\sum_{q'}e^{i\omega_{cp,aq'}t}B_{cp,aq'}(\mathbf{k})\rho^I_{aq';aq}\\-\sum_{p'}e^{i\omega_{cp',aq}t}\rho^I_{cp;cp'}B_{cp',aq}(\mathbf{k})\end{bmatrix}, \tag{7b}$$

$$\dot{\rho}^I_{cp;cp'} = -i\frac{\Omega_{ca}(t)}{2}\sum_q \begin{bmatrix} e^{i\omega_{cp,aq}t}B_{cp,aq}(\mathbf{k})\rho^I_{aq;cp'} \\ -e^{-i\omega_{cp',aq}t}\rho^I_{cp;aq}B^\dagger_{aq,cp'}(\mathbf{k}) \end{bmatrix}, \tag{7c}$$

$$\dot{\rho}^I_{aq;aq'} = -i\frac{\Omega_{ca}(t)}{2}\sum_p \begin{bmatrix} e^{i\omega_{aq,cp}t}B^\dagger_{aq,cp}(\mathbf{k})\rho^I_{cp;aq'} \\ -e^{-i\omega_{aq',cp}t}\rho^I_{aq;cp}B_{cp,aq'}(\mathbf{k}) \end{bmatrix}, \tag{7d}$$

where $\mathbf{k} = k\mathbf{u}_x$ and

$$B_{cp,aq}(\mathbf{k}) = \int d\mathbf{R}[\psi_{cp}(\mathbf{R})]^* f(\mathbf{R})e^{i\mathbf{k}\cdot\mathbf{R}}\psi_{aq}(\mathbf{R}), \tag{8a}$$

$$B^\dagger_{aq,cp}(\mathbf{k}) = \int d\mathbf{R}[\psi_{aq}(\mathbf{R})]^* f(\mathbf{R})e^{-i\mathbf{k}\cdot\mathbf{R}}\psi_{cp}(\mathbf{R}). \tag{8b}$$

If we define an operator

$$M_{ca}(\mathbf{R},\mathbf{k},t) = f(\mathbf{R})e^{iH_c(\mathbf{R})t/\hbar}e^{i\mathbf{k}\cdot\mathbf{R}}e^{-iH_a(\mathbf{R})t/\hbar}, \tag{9}$$

then Eqs. (7) can be written in matrix form as

$$\dot{\rho}^I_{ac} = -i\frac{\Omega_{ca}(t)}{2}\big[M_{ca}(\mathbf{k},t)^\dagger\rho^I_{cc} - \rho^I_{aa}M_{ca}(\mathbf{k},t)^\dagger\big], \tag{10a}$$

$$\dot{\rho}^I_{ca} = -i\frac{\Omega_{ca}(t)}{2}\big[M_{ca}(\mathbf{k},t)\rho^I_{aa} - \rho^I_{cc}M_{ca}(\mathbf{k},t)\big], \tag{10b}$$

$$\dot{\rho}^I_{cc} = -i\frac{\Omega_{ca}(t)}{2}\big[M_{ca}(\mathbf{k},t)\rho^I_{ac} - \rho^I_{ca}M_{ca}(\mathbf{k},t)^\dagger\big], \tag{10c}$$

$$\dot{\rho}^I_{aa} = -i\frac{\Omega_{ca}(t)}{2}\big[M_{ca}(\mathbf{k},t)^\dagger\rho^I_{ca} - \rho^I_{ac}M_{ca}(\mathbf{k},t)\big], \tag{10d}$$

where each element $\rho^I_{\alpha\alpha'}$ is now a *matrix* having matrix elements $\langle\alpha q|\rho^I_{\alpha\alpha'}|\alpha' q'\rangle$ and M_{ca} is a matrix with elements

$$[M_{ca}(\mathbf{k},t)]_{\alpha q;\beta q'} = \langle\alpha q|M_{ca}(\mathbf{R},\mathbf{k},t)|\beta q'\rangle \tag{11}$$

for α, β equal to a or c. The pulse duration is sufficiently short to neglect any decay during the pulse. Note that $M_{ca}(\mathbf{R},\mathbf{k},t)$ is *not* a unitary operator owing to the factor $f(\mathbf{R})$, but that the operator

$$U_{ca}(\mathbf{R},\mathbf{k},t) = e^{iH_c(\mathbf{R})t/\hbar}e^{i\mathbf{k}\cdot\mathbf{R}}e^{-iH_a(\mathbf{R})t/\hbar} \tag{12}$$

is unitary.

In principle, Eqs. (10) could be solved numerically as coupled equations for all the matrix elements. However, if the pulse duration T_p is sufficiently short such that $|\omega_{aq,cp}T_p| \ll 1$ for all relevant q and p (this corresponds to the atomic motion being frozen during the pulse), then the matrix $M_{ca}(\mathbf{k},t)$ can be evaluated at $t = t_n$ and Eqs. (10) reduce to

$$\dot{\rho}^I_{ac} = -i\frac{\Omega_{ca}(t)}{2}\big[M_{ca}(\mathbf{k},t_n)^\dagger\rho^I_{cc} - \rho^I_{aa}M_{ca}(\mathbf{k},t_n)^\dagger\big], \tag{13a}$$

$$\dot{\rho}^I_{ca} = -i\frac{\Omega_{ca}(t)}{2}\big[M_{ca}(\mathbf{k},t_n)\rho^I_{aa} - \rho^I_{cc}M_{ca}(\mathbf{k},t_n)\big], \tag{13b}$$

$$\dot{\rho}^I_{cc} = -i\frac{\Omega_{ca}(t)}{2}\big[M_{ca}(\mathbf{k},t_n)\rho^I_{ac} - \rho^I_{ca}M_{ca}(\mathbf{k},t_n)^\dagger\big], \tag{13c}$$

$$\dot{\rho}^I_{aa} = -i\frac{\Omega_{ca}(t)}{2}\big[M_{ca}(\mathbf{k},t_n)^\dagger\rho^I_{ca} - \rho^I_{ac}M_{ca}(\mathbf{k},t_n)\big]. \tag{13d}$$

Unfortunately, even though $M_{ca}(\mathbf{k},t_n)$ and $M_{ca}(\mathbf{k},t_n)^\dagger$ are time independent in these equations, there is no simple solution owing to the fact that $M_{ca}(\mathbf{k},t_n)$ is not a unitary matrix. In effect, Eqs. (10) must be solved numerically to obtain the $\rho^I_{\alpha q;\beta q'}(t_n^+)$ in terms of $\rho^I_{\alpha q,\beta q'}(t_n^-)$.

There are two limiting cases where a relatively simple solution can be obtained. If the applied field spatial profile is constant over the sample [$f(\mathbf{R})=1$ and $M_{ca}(\mathbf{k},t_n)=U_{ca}(\mathbf{k},t_n)$], then we can set

$$\tilde{\rho}_{ac}(\mathbf{k},t,t_n) = \rho^I_{ac}(t)U_{ca}(\mathbf{k},t_n), \tag{14a}$$

$$\tilde{\rho}_{ca}(\mathbf{k},t,t_n) = U_{ca}(\mathbf{k},t_n)^\dagger\rho^I_{ca}(t), \tag{14b}$$

$$\tilde{\rho}_{aa}(\mathbf{k},t,t_n) = \rho^I_{aa}(t), \tag{14c}$$

$$\tilde{\rho}_{cc}(\mathbf{k},t,t_n) = U_{ca}(\mathbf{k},t_n)^\dagger\rho^I_{cc}(t)U_{ca}(\mathbf{k},t_n), \tag{14d}$$

which transforms Eqs. (13) into

$$\frac{d\tilde{\rho}_{ac}}{dt} = -i\frac{\Omega_{ca}(t)}{2}[\tilde{\rho}_{cc} - \tilde{\rho}_{aa}], \tag{15a}$$

$$\frac{d\tilde{\rho}_{ca}}{dt} = -i\frac{\Omega_{ca}(t)}{2}[\tilde{\rho}_{aa} - \tilde{\rho}_{cc}], \tag{15b}$$

$$\frac{d\tilde{\rho}_{cc}}{dt} = -i\frac{\Omega_{ca}(t)}{2}[\tilde{\rho}_{ac} - \tilde{\rho}_{ca}], \tag{15c}$$

$$\frac{d\tilde{\rho}_{aa}}{dt} = -i\frac{\Omega_{ca}(t)}{2}[\tilde{\rho}_{ca} - \tilde{\rho}_{ac}]. \tag{15d}$$

The solution of these equations is straightforward [22]

$$\begin{pmatrix} \tilde{\rho}_{ac}(t_n^+) \\ \tilde{\rho}_{ca}(t_n^+) \\ \tilde{\rho}_{aa}(t_n^+) \\ \tilde{\rho}_{cc}(t_n^+) \end{pmatrix} = \begin{pmatrix} \cos^2\left(\frac{A}{2}\right) & \sin^2\left(\frac{A}{2}\right) & i\frac{\sin A}{2} & -i\frac{\sin A}{2} \\ \sin^2\left(\frac{A}{2}\right) & \cos^2\left(\frac{A}{2}\right) & -i\frac{\sin A}{2} & i\frac{\sin A}{2} \\ i\frac{\sin A}{2} & -i\frac{\sin A}{2} & \cos^2\left(\frac{A}{2}\right) & \sin^2\left(\frac{A}{2}\right) \\ -i\frac{\sin A}{2} & i\frac{\sin A}{2} & \sin^2\left(\frac{A}{2}\right) & \cos^2\left(\frac{A}{2}\right) \end{pmatrix} \times \begin{pmatrix} \tilde{\rho}_{ac}(t_n^-) \\ \tilde{\rho}_{ca}(t_n^-) \\ \tilde{\rho}_{aa}(t_n^-) \\ \tilde{\rho}_{cc}(t_n^-) \end{pmatrix}, \tag{16}$$

where $t_n^\pm$ are times just before and after the application of the pulse and

$$A = \int_{t_n^-}^{t_{n+}} dt\,\Omega_{ca}(t) \tag{17}$$

is a pulse area. Equations (16) and (14) can be used to calculate the change in the atomic density matrix elements in the interaction representation.

The second case where a simple solution is possible is one in which there is a lattice trap potential varying as $-V_0\cos^2(k_{tr}X)$ superimposed on a much more slowly varying trap potential. If the temperature is sufficiently low to ensure that all atomic motion can be neglected on the timescale of an experiment *except* that associated with motion in the lattice potential, but is still sufficiently large to ensure that motion in the slowly varying trap potential can be treated classically, then $f(\mathbf{R})$ can be replaced by a classical function $f_{cl}(\mathbf{R})$ and the resulting signal averaged over the classical Boltzmann distribution associated with the slowly varying

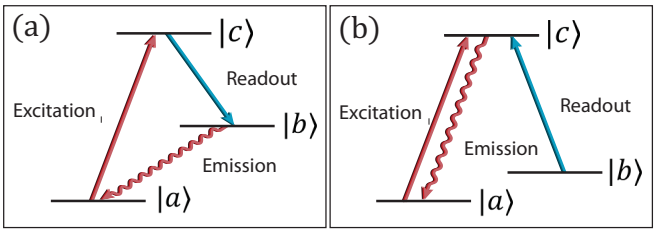

FIG. 1. Level schemes.

trap potential. In this limit, Eqs. (14) and (16) remain valid, provided that the area A appearing in Eq. (16) is replaced by

$$A(\mathbf{R}) = f_{cl}(\mathbf{R}) \int_{t_n^-}^{t_n^+} dt\, \Omega_{ca}(t). \tag{18}$$

Although we have taken the a-c transition to be dipole allowed, the formalism can still be used when levels a and c have the same parity and are driven by two-photon excitation. The only change that need be made is to replace $\Omega_{ca}(t)$ by some effective two-photon Rabi frequency that depends on the product of the amplitudes of each of the fields involved in the transition.

B. Readout pulse

In some cases, it is necessary to apply a readout pulse to generate the phase-matched signal. For example, consider the level schemes shown in Fig. 1. In both cases, it is assumed that some initial two-photon pulse has created a long-lived atomic coherence between levels a and c, both of which have the same parity. In Fig. 1(a), the coherence is between a ground and Rydberg level and, in Fig. 1(b), it is between two-ground state sublevels. To read out the coherence, a pulse is applied that is resonant with the c-b transition and results in phase-matched emission on the a-b transition. We shall assume that the Rabi frequency $\Omega_{bc}^{\rm out}$ associated with the readout pulse is greater than the decay rate $\Gamma_b = 2\gamma_b$ of level b. The duration $T_{\rm out}$ of the readout pulse may be greater than Γ_b^{-1}; it is assumed, however, that all motion is frozen on a timescale of min $(\gamma_b^{-1}, T_{\rm out})$.

The calculation proceeds in exactly the same manner as that for the excitation pulse, except it is necessary to use density matrix equations for a three-level lambda scheme [23] with a single field acting on the c-b transition. We find that, for the level scheme of Fig. 1(a) and $f(\mathbf{R}) = 1$,

$$\frac{d\tilde{\rho}_{ca}}{dt} = -i\frac{\Omega_{cb}^{\rm out}(t)}{2}\tilde{\rho}_{ba}, \tag{19a}$$

$$\frac{d\tilde{\rho}_{ba}}{dt} = -i\frac{\Omega_{cb}^{\rm out}(t)}{2}\tilde{\rho}_{ca} - \gamma_b\tilde{\rho}_{ba}, \tag{19b}$$

where

$$\tilde{\rho}_{ca}(\mathbf{k}_n, t, t_{\rm out}) = U_{cb}(\mathbf{k}_{\rm out}, t_{\rm out})^\dagger \rho_{ca}^I(t), \tag{20a}$$

$$\tilde{\rho}_{ba}(\mathbf{k}_n, t, t_{\rm out}) = \rho_{ba}^I(t), \tag{20b}$$

$\mathbf{k}_{\rm out}$ is the propagation vector of the readout pulse, and $t_{\rm out}$ is the time the readout pulse is applied.

For the level scheme of Fig. 1(b) and $f(\mathbf{R}) = 1$,

$$\frac{d\tilde{\rho}_{ca}}{dt} = -i\frac{\Omega_{bc}^{\rm out}(t)}{2}\tilde{\rho}_{ba}, \tag{21a}$$

$$\frac{d\tilde{\rho}_{ba}}{dt} = -i\frac{\Omega_{bc}^{\rm out}(t)}{2}\tilde{\rho}_{ca} - \gamma_b\tilde{\rho}_{ba}, \tag{21b}$$

where

$$\tilde{\rho}_{ca}(\mathbf{k}_n, t, t_{\rm out}) = U_{cb}(\mathbf{k}_{\rm out}, t_{\rm out})\rho_{ca}^I(t), \tag{22a}$$

$$\tilde{\rho}_{ba}(\mathbf{k}_n, t, t_{\rm out}) = \rho_{ba}^I(t). \tag{22b}$$

It is a simple matter to solve Eqs. (19) or (21) numerically (or analytically for a square pulse) and then use Eqs. (20) or (22) to obtain matrix elements of $\rho_{ca}^I(t)$, matrix elements that will be needed in the evaluation of the phase-matched signal. If, instead of taking $f(\mathbf{R}) = 1$, we consider the second limiting case discussed following Eq. (13), then $\Omega_{bc}^{\rm out}(t)$ is replaced by $\Omega_{bc}^{\rm out}(t) f_{cl}(\mathbf{R})$ in Eqs. (19) and (21).

III. SOURCE-FIELD EXPRESSION FOR THE SIGNAL

The signal recorded at time t at a point detector located at position $\mathbf{R}_d$ is proportional to a quantity S defined by

$$S = R_d^2 \langle \mathbf{E}_-(\mathbf{R}_d, t) \cdot \mathbf{E}_+(\mathbf{R}_d, t)\rangle, \tag{23}$$

where

$$\mathbf{E}_+(\mathbf{R}, t) = i\sum_{\mathbf{k},\lambda}\left(\frac{\hbar\omega_k}{2\epsilon_0\mathcal{V}}\right)^{1/2} e^{i\mathbf{k}\cdot\mathbf{R}} a_{\mathbf{k}_\lambda}(t)\boldsymbol{\epsilon}_{\mathbf{k}}^{(\lambda)} \tag{24}$$

is the positive-frequency component of the electric field operator at position $\mathbf{R}_d$, $\mathbf{E}_-(\mathbf{R}_d, t) = [\mathbf{E}_+(\mathbf{R}, t)]^\dagger$, $\omega_k = kc$,

$$\boldsymbol{\epsilon}_{\mathbf{k}}^{(1)} = \cos\theta_k \cos\phi_k \mathbf{u}_x + \cos\theta_k \sin\phi_k \mathbf{u}_y - \sin\theta_k \mathbf{u}_z, \tag{25a}$$

$$\boldsymbol{\epsilon}_{\mathbf{k}}^{(2)} = -\sin\phi_k \mathbf{u}_x + \cos\phi_k \mathbf{u}_y \tag{25b}$$

are the field polarization vectors labeled by the symbol λ, and $\mathcal{V}$ is the quantization volume. The field operators are written in the Heisenberg representation, but could have equally well been written as time-independent operators in the Schrödinger representation. We will return to this point shortly.

In the problem under consideration, a number of classical field pulses give rise to the creation of previously unoccupied vacuum field modes. In situations such as this, a powerful method for obtaining an expression for $\mathbf{E}_+(\mathbf{R}_d, t)$ is afforded by the so-called source-field approach [21]. In that approach, the creation and annihilation operators are written in terms of their initial values and their dependence on atomic operators. For example, consider emission on transitions from level b to a having transition frequency ω_{ba} in an ensemble of atoms whose center-of-mass coordinates are fixed. Level b is taken to be the $m = 0$ sublevel of a $J = 1$ angular momentum state, while level a is taken to be a $J = 0$ angular momentum state. In that case, for an electric dipole interaction of the form

$$V_{af}(\mathbf{R}, t) = -\hat{\boldsymbol{\mu}}(t) \cdot [\mathbf{E}_+(\mathbf{R}, t) + \mathbf{E}_-(\mathbf{R}, t)], \tag{26}$$

where $\hat{\boldsymbol{\mu}}(t)$ is the atomic dipole moment operator, the Hamiltonian in the RWA is given by

$$H = \hbar\omega_a|a\rangle\langle a| + \hbar\omega_b|b\rangle\langle b| + \sum_{\mathbf{k},\lambda}\sum_{j=1}^{N}\begin{bmatrix}\hbar g_{\mathbf{k}_\lambda} e^{i\mathbf{k}\cdot\mathbf{R}_j} e^{-i\omega_k t}\sigma_{ba}^{(j)}(t)a_{\mathbf{k}_\lambda}(t) \\ +\hbar g_{\mathbf{k}_\lambda}^{*} e^{-i\mathbf{k}\cdot\mathbf{R}_j} e^{i\omega_k t} a_{\mathbf{k}_\lambda}^{\dagger}(t)\sigma_{ab}^{(j)}(t)\end{bmatrix}, \tag{27}$$

where

$$g_{\mathbf{k}_\lambda} = -i\mu_{ba}\left(\frac{\omega_k}{2\hbar\epsilon_0\mathcal{V}}\right)^{1/2}\sin\theta_k\delta_{\lambda,1}, \tag{28}$$

$\sigma_{ab}^{(j)}(t')$ [$\sigma_{ba}^{(j)}(t')$] is a lowering (raising) operator for atom j located at position $\mathbf{R}_j$, μ_{ba} is the z component of the dipole moment matrix element (assumed real) between states b and a, and $\delta_{\lambda,1}$ is a Kronecker delta. The annihilation operator at time t can be expressed as

$$a_{\mathbf{k}_\lambda}(t) = a_{\mathbf{k}_\lambda}(0)e^{-i\omega_k t} - ig_{\mathbf{k}_\lambda}^{*}\sum_{j=1}^{N}\int_0^t dt' e^{-i\mathbf{k}\cdot\mathbf{R}_j}\sigma_{ab}^{(j)}(t')e^{-i\omega_k(t-t')}. \tag{29}$$

The second term in Eq. (29) is the contribution to the field operator that can be traced to the atoms, the so-called source-field term. Including only the source-field contribution in Eq. (24), it is straightforward to show that the field operator can be written in a form that mirrors the classical expression for the electric field produced by an ensemble of electric dipoles. In particular, assuming that the detector is located in the radiation zone of the atomic dipoles, one finds [21]

$$\mathbf{E}_+(\mathbf{R}_d,t) = -\left(\frac{\omega_{ba}^2}{4\pi\epsilon_0 c^2 R_d}\right)\mu_{ba}\sin\theta_d\sum_{j=1}^{N}\sigma_{ab}^{(j)}\left(t_r^{(j)}\right)\mathbf{u}_{\theta_d}, \tag{30}$$

where θ_d is the polar angle of the detector, $\mathbf{u}_{\theta_d}$ is a unit vector in the direction of increasing θ_d, and

$$t_r^{(j)} = t - \frac{|\mathbf{R}_d - \mathbf{R}_j|}{c} \tag{31}$$

is a retarded time.

If the center-of-mass motion of the atoms can be treated *classically*, it is a simple matter to extend the source-field result to include the effects of atomic motion. Equation (30) remains valid provided that $t_r^{(j)}$ is defined as the solution of

$$t_r^{(j)} = t - \frac{\left|\mathbf{R}_d - \mathbf{R}_j\left(t_r^{(j)}\right)\right|}{c}, \tag{32}$$

where $\mathbf{R}_j(t)$ is the position of atom j at time t. On the other hand, if the center-of-mass motion of the atoms is quantized, $\mathbf{R}_j(t)$ becomes a Heisenberg *operator*, and there is no obvious manner in which to generalize Eq. (30).

To make some progress in the case where the center-of-mass motion is quantized, we can still use the Heisenberg representation, but it is necessary to delay the sum over field modes that lead to the final source-field expression. In other words, we use Eqs. (23) and (28) with R_j replaced by $R_j(t')$ to write the source-field contribution to the signal as

$$\begin{aligned} S &= R_d^2\langle\mathbf{E}_-(\mathbf{R}_d,t)\cdot\mathbf{E}_+(\mathbf{R}_d,t)\rangle \\ &= R_d^2\sum_{\mathbf{k},\lambda,\mathbf{k}',\lambda'}\left(\frac{\hbar\omega_{k'}}{2\epsilon_0\mathcal{V}}\right)^{1/2}\left(\frac{\hbar\omega_k}{2\epsilon_0\mathcal{V}}\right)^{1/2}e^{i(\mathbf{k}-\mathbf{k}')\cdot\mathbf{R}_d} \\ &\quad\times\left\langle a_{\mathbf{k}'_{\lambda'}}^{\dagger}(t)a_{\mathbf{k}_\lambda}(t)\right\rangle\boldsymbol{\epsilon}_{\mathbf{k}'}^{(\lambda')}\cdot\boldsymbol{\epsilon}_{\mathbf{k}}^{(\lambda)} \\ &= \mu_{ba}^2 R_d^2\sum_{\mathbf{k},\mathbf{k}'}\sum_{j,j'=1}^{N}\left(\frac{\hbar\omega_{k'}}{2\epsilon_0\mathcal{V}}\right)\left(\frac{\hbar\omega_k}{2\epsilon_0\mathcal{V}}\right) \\ &\quad\times\sin\theta_k\sin\theta_{k'}e^{i(\mathbf{k}-\mathbf{k}')\cdot\mathbf{R}_d}\boldsymbol{\epsilon}_{\mathbf{k}'}^{(1)}\cdot\boldsymbol{\epsilon}_{\mathbf{k}}^{(1)} \\ &\quad\times\int_0^t dt'\int_0^t dt''\left\langle e^{i\mathbf{k}'\cdot\hat{\mathbf{R}}_{j'}(t'')}\sigma_{ba}^{(j')}(t'')\sigma_{ab}^{(j)}(t')e^{-i\mathbf{k}\cdot\hat{\mathbf{R}}_j(t')}\right\rangle \\ &\quad\times e^{i\omega_{k'}(t-t')}e^{-i\omega_k(t-t')}, \end{aligned} \tag{33}$$

where $\hat{\mathbf{R}}_j(t)$ is a Heisenberg operator. Note that $[\hat{\mathbf{R}}_j(t),\sigma_{\alpha\beta}^{(j)}(t)] = 0$, but that $[\hat{\mathbf{R}}_j(t),\sigma_{\alpha\beta}^{(j)}(t')] \neq 0$, in general.

Qualitatively, there are two types of terms that enter the double summation over j and j' in Eq. (33). Terms with $j = j'$ are difficult to calculate using this approach, but such terms contribute negligibly to the phase-matched signal. For completeness, a method for treating the $j = j'$ terms is discussed in the Appendix. The remaining terms involve products of operators corresponding to different atoms, implying that the average of the product is equal to the product of the averages. In other words, for such terms we can write Eq. (33) as

$$S = |G(\mathbf{R}_d,t)|^2, \tag{34}$$

where

$$G(\mathbf{R}_d,t) = \mu_{ba}R_d\sum_{\mathbf{k},\mathbf{k}'}\sum_{j=1}^{N}\left(\frac{\hbar\omega_k}{2\epsilon_0\mathcal{V}}\right)\int_0^t dt'\left\langle\sigma_{ab}^{(j)}(t')e^{-i\mathbf{k}\cdot\hat{\mathbf{R}}_j(t')}\right\rangle \times e^{-i\omega_k(t-t')}. \tag{35}$$

Written in this form, the signal contains extra terms since terms with $j = j'$ are not excluded; however, for a large number of atoms N in the sample, the $j = j'$ terms can be neglected since they scale as N, whereas the phase-matched signal scales as N^2.

The average in Eq. (35) can be written as

$$\begin{aligned} F_j &= \left\langle\sigma_{ab}^{(j)}(t')e^{-i\mathbf{k}\cdot\hat{\mathbf{R}}_j(t')}\right\rangle = \mathrm{Tr}\left[\rho(0)\sigma_{ab}^{(j)}(t')e^{-i\mathbf{k}\cdot\hat{\mathbf{R}}_j(t')}\right] \\ &= \mathrm{Tr}\left[\rho^{(j)}(t')|a\rangle\langle b|e^{-i\mathbf{k}\cdot\hat{\mathbf{R}}_j}\right], \end{aligned} \tag{36}$$

where $\rho^{(j)}(t)$ is the density matrix for atom j at time t and the trace is over motional states. The trace is very difficult to carry out using Heisenberg operators, but relatively simple to evaluate using Schrödinger operators. Explicitly, we find

$$\begin{aligned} F_j &= \sum_{q,q'}\rho_{bq;aq'}^{(j)}(t')\langle aq'|e^{-i\mathbf{k}\cdot\hat{\mathbf{R}}_j}|bq\rangle \\ &= \sum_{q,q'}\rho_{bq;aq'}^{I(j)}(t')\langle aq'|e^{-i\mathbf{k}\cdot\hat{\mathbf{R}}_j}|bq\rangle e^{-i\omega_{bq;aq'}t'}e^{-i\omega_{ba}t'} \\ &= \sum_{q,q'}\int d\mathbf{R}\left[\psi_{aq'}^{(j)}(\mathbf{R})\right]^{*}e^{-i\mathbf{k}\cdot\mathbf{R}}\psi_{bq}^{(j)}(\mathbf{R})\rho_{bq;aq'}^{I(j)}(t') \\ &\quad\times e^{-i\omega_{bq;aq'}t'}e^{-i\omega_{ba}t'}. \end{aligned} \tag{37}$$

The key point is that the **R** appearing in Eq. (37) is no longer an operator. As a consequence, when this expression is substituted back into Eq. (35), the sum over field modes can be carried out as in normal source-field theory. In this manner, we find

$$G(\mathbf{R}_d,t) = -\mu_{ba}\left(\frac{\omega_{ba}^2\sin\theta_d}{4\pi\epsilon_0 c^2}\right)\sum_{q,q'}\sum_{j=1}^{N}\int d\mathbf{R}\big[\psi_{aq'}^{(j)}(\mathbf{R})\big]^* \times \rho_{bq;aq'}^{I(j)}\left(t-\frac{|\mathbf{R}_d-\mathbf{R}|}{c}\right) \times \exp\left[-i\omega_{bq;aq'}\left(t-\frac{|\mathbf{R}_d-\mathbf{R}|}{c}\right)\right] \times \exp\left[-i\omega_{ba}\left(t-\frac{|\mathbf{R}_d-\mathbf{R}|}{c}\right)\right]\psi_{bq}^{(j)}(\mathbf{R}). \quad (38)$$

Since $R_d \gg R$ we can set $|\mathbf{R}_d-\mathbf{R}| = R_d$ *except* in the exponential containing ω_{ba} since ω_{ba} corresponds to an optical frequency. In that term, we set

$$|\mathbf{R}_d-\mathbf{R}| \approx R_d - \frac{\mathbf{R}_d\cdot\mathbf{R}}{R_d} \quad (39)$$

and Eq. (38) reduces to

$$G(\mathbf{R}_d,t) = -\mu_{ba}\left(\frac{\omega_{ba}^2\sin\theta_d}{4\pi\epsilon_0 c^2}\right)e^{ik_{ba}R_d}e^{-i\omega_{ba}t} \times \sum_{q,q'}\sum_{j=1}^{N}\rho_{bq;aq'}^{I(j)}(t_r)U_{aq',bq}^{(j)}(\mathbf{k}_{ba},t_r)^\dagger, \quad (40)$$

where

$$U_{aq',bq}^{(j)}(\mathbf{k}_{ba},t_r)^\dagger = e^{-i\omega_{bq;aq'}t_r}\int d\mathbf{R}\big[\psi_{aq'}^{(j)}(\mathbf{R})\big]^* e^{-i\mathbf{k}_{ba}\cdot\mathbf{R}}\psi_{bq}^{(j)}(\mathbf{R}), \quad (41)$$

$$\mathbf{k}_{ba} = \frac{\omega_{ba}}{c}\frac{\mathbf{R}_d}{R_d}, \quad (42)$$

and

$$t_r = t - R_d/c. \quad (43)$$

Equation can be written in the more compact form as

$$G(\mathbf{R}_d,t) = -\mu_{ba}\left(\frac{\omega_{ba}^2\sin\theta_d}{4\pi\epsilon_0 c^2}\right)e^{ik_{ba}R_d}e^{-i\omega_{ba}t} \times \sum_{j=1}^{N}\mathrm{Tr}\big[\rho_{ba}^{I(j)}(t_r)U_{ba}^{(j)}(\mathbf{k}_{ba},t_r)^\dagger\big], \quad (44)$$

where both $\rho_{ba}^{I(j)}(t_r)$ and $U_{ba}^{(j)}(\mathbf{k},t_r)^\dagger$ are matrices in the motional states. Recall that $U_{ba}(\mathbf{R},\mathbf{k},t_r)$ is defined in Eq. (12). The trace in Eq. (44) is over center-of-mass states. Although we have retained the j superscripts in Eq. (44), the final result is actually equal to N times the single-atom result since each atom in our model is essentially the same.

In principle, the calculation is now complete. One calculates $\rho_{ba}^{I(j)}(t_r)$ by piecing together the various transfer matrices calculated using the method outlined in Sec. II and then carries out the trace needed in Eq. (44). As specific examples, we now calculate the signal associated with the level schemes of Fig. 1.

IV. SPECIFIC EXAMPLE: GROUND LEVEL–RYDBERG LEVEL COHERENCE IN AN OPTICAL LATTICE

We consider first the level scheme of Fig. 1(a) in which level a is a $J=0$ ground state, level c is a $J=0$ Rydberg level, and level b is a $J=1$ excited state. Trap fields, counterpropagating in the X direction and polarized in the y direction, confine the atoms in the transverse direction and provide attractive lattice potentials

$$V_\alpha(X) = -V_\alpha\cos^2(k_{tr}X), \quad \alpha = a,c \quad (45)$$

in the longitudinal (X) direction for levels a and c. Any additional contributions to the trap potentials, such as those associated with a breakdown of the dipole approximation in calculating the Rydberg potentials [24], are ignored. The trap fields can also give rise to a repulsive potential for level b, but we will see that the potential for level b is unimportant for the pulse sequence under consideration. At $t=0$, a two-photon pulse resonantly excites atomic coherences $\rho_{ca}^{(j)}$. As a result of atomic motion, these coherences undergo dephasing. At time $t=T_{21}$, a readout pulse that is resonant with the c-b transition frequency is applied and creates the coherences $\rho_{ba}^{(j)}$. The phase-matched signal emitted by the sample, which results from the interaction of the vacuum field with the atoms, is dependent on the value of $\rho_{ba}^{(j)}$ created by the excitation and readout fields.

The excitation and readout pulses are all z polarized and propagate in the $\pm X$ direction. The two-photon excitation pulse consists of two fields having propagation vectors $\mathbf{k}_1 = k_1\mathbf{u}_x$ and $\mathbf{k}_2 = -k_2\mathbf{u}_x$. The excitation pulse has an effective propagation vector $\mathbf{k}_e = \mathbf{k}_{12} = k_{12}\mathbf{u}_x$, where

$$k_{12} = k_1 - k_2, \quad (46)$$

an effective two-photon frequency $\omega_e = (|k_1|+|k_2|)c = \omega_{ca}$, and an effective two-photon Rabi frequency $\Omega_{ca}(t)$, while the readout pulse has propagation vector $\mathbf{k}_{\rm out}$, frequency $\omega_{\rm out} = \omega_{cb}$, and Rabi frequency $\Omega_{cb}(t)$. The waists of the excitation and readout pulses are centered at the center of the atomic cloud at times $t=0$ and T_{21}, respectively. The trap fields are also centered at the center of the atomic cloud. It is assumed that the radial extent of the excitation field is much smaller than that of the trap fields and that the trap-field intensity in the longitudinal direction is constant over the extent of the atomic cloud. As a consequence, the trap fields can be taken to be constant over the excitation volume. Moreover, we assume that the atoms are sufficiently cold that any *transverse* motion can be neglected on a timescale equal to T_{21}. For example, if the atoms are cooled to 10 μK, they move a distance of order 1.8 μm in 40 μs. For T_{21} of order 40 μs, the transverse motion can be neglected if the waist of the excitation pulse is much greater than 1.8 μm. The pulse durations are sufficiently short to neglect *all* motion during the pulses. With these simplifying assumptions, the atomic density $\mathcal{N}$ can be taken as constant over the excitation volume and the spatial profiles of the excitation and readout pulses can be considered as *classical* functions of atomic position.

The problem effectively reduces to a one-dimensional problem for quantized motion in potentials

$$V_\alpha(X) = -V_\alpha \cos^2(k_{tr}X) = -V_\alpha + V_\alpha \sin^2(k_{tr}X), \quad \alpha = a, c. \tag{47}$$

It proves convenient to set

$$V_\alpha = \frac{1}{2}\frac{M\tilde{\omega}_\alpha^2}{k_{tr}^2}, \quad \alpha = a, c \tag{48}$$

where M is the mass of the atoms, with this definition the motion near the bottom of the wells is approximately harmonic with frequency $\tilde{\omega}_\alpha$. We assume that all the atoms in the excitation volume are trapped in the lattice wells; transitions out of the wells are not included.

The evaluation of Eq. (44) for $G(\mathbf{R}_d, t)$ is complicated since it is necessary to use the quasibound eigenfunctions of the trap potential. For a potential having N_p lobes, the ground state (and each excited quasibound state) is approximately N_p-fold degenerate. Of the N_p-degenerate eigenfunctions, only *two* correspond to the periodic Mathieu functions; the remaining states are symmetric or antisymmetric eigenfunctions of the N_p-well potential [25]. Instead of using these eigenfunctions, we assume atoms are trapped in individual wells of the potential with no coherence between the wave functions of the atoms in different wells. As such, the motional quantum numbers are simply those associated with the quasibound states of a single lobe of the lattice potential. It is now a simple matter to piece together the signal.

Using Eq. (16), we find that the excitation pulse results in a density matrix

$$\tilde{\rho}_{ca}^{(j)}(0^+) = -i\frac{\sin[A_e(\boldsymbol{\rho})]}{2}\tilde{\rho}_{aa}^{(j)}(0^-), \tag{49}$$

where

$$A_e(\boldsymbol{\rho}) = f_e(\boldsymbol{\rho})\int_{0^-}^{0^+} dt\, \Omega_{ca}(t), \tag{50}$$

$\boldsymbol{\rho}$ is a vector orthogonal to the X axis, and $f_e(\boldsymbol{\rho})$ is the (classical) transverse spatial profile of the excitation pulse, which is the same for all atoms in the excitation volume. From Eqs. (14b) and (14c), it then follows that

$$\rho_{ca}^{I(j)}(0^+) = U_{ca}^{(j)}(k_{12}\mathbf{u}_x, 0)\tilde{\rho}_{ca}^{(j)}(0^+). \tag{51}$$

Between $t = 0$ and T_{21}, this coherence decays as a result of loss of population from level c with rate Γ_c, such that

$$\rho_{ca}^{I(j)}(T_{21}^-) = e^{-\gamma_c T_{21}}\rho_{ca}^{I(j)}(0^+), \tag{52}$$

where $\gamma_c = \Gamma_c/2$. At time $t_{\rm out} = T_{21}$, the readout pulse transforms the c-a coherence into a b-a coherence which can be calculated using Eqs. (16) and (20) as

$$\rho_{ba}^{I(j)}(T_{21}^+) = \tilde{\rho}_{ba}^{(j)}(T_{21}^+) = -i\frac{\sin[A_{\rm out}(\boldsymbol{\rho})]}{2}\tilde{\rho}_{ca}^{(j)}(T_{21}^-) = -i\frac{\sin[A_{\rm out}(\boldsymbol{\rho}]}{2}U_{cb}^{(j)}(-k_2\mathbf{u}_x, T_{21})^\dagger\rho_{ca}^{I(j)}(T_{21}^-), \tag{53}$$

where

$$A_{\rm out}(\boldsymbol{\rho}) = f_{\rm out}(\boldsymbol{\rho})\int_{T_{21}^-}^{T_{21}^+} dt\, \Omega_{cb}(t), \tag{54}$$

and $f_{\rm out}(\boldsymbol{\rho})$ is the transverse spatial profile of the readout pulse. For times $t > T_{21}^+$,

$$\rho_{ba}^{I(j)}(t) = e^{-\gamma_b(t-T_{21})}\rho_{ba}^{I(j)}(T_{21}^+), \tag{55}$$

where $\gamma_b = \Gamma_b/2$ and Γ_b is the rate at which the level b population decays.

The detector is located at position $\mathbf{R}_d = R_d\mathbf{u}_x$, which is in the direction of phase-matched emission. As a consequence, the vector $\mathbf{k}_{ba}$ appearing in Eq. (40) is

$$\mathbf{k}_{ba} = (\omega_{ba}/c)\mathbf{u}_x = k_1\mathbf{u}_x. \tag{56}$$

To achieve phase matching, it is necessary that $|k_2 - k_{\rm out}|L \ll 1$, as is assumed ($L$ is the longitudinal length of the sample). In calculating $G(\mathbf{R}_d, t)$, given in Eq. (44), several factors of $U_{\alpha\beta}^{(j)}(k\mathbf{u}_x, T_{21})$ or its adjoint appear. Using the fact that atom j is in a potential well centered at $X = X_j$, it follows from Eq. (41) that

$$U_{aq',bq}^{(j)}(k\mathbf{u}_x, t_r) = e^{ikX_j}U_{aq',bq}^{(j)}(k\mathbf{u}_x, t_r), \tag{57}$$

where

$$U_{aq',bq}(k\mathbf{u}_x, t_r) = e^{i\omega_{bq;aq'}t_r}\int dX[\psi_{aq'}(X)]^* e^{ikX}\psi_{bq}(X) \tag{58}$$

is independent of j and the integral is carried out over a single well centered at $X = 0$. The resulting exponential factors in the expression for $G(\mathbf{R}_d, t)$ are equal to unity in the phase-matched direction. As a consequence, we can combine Eqs. (34), (44), and (49)–(56) to find that the phase-matched contribution to the signal S emitted on the b-a transition at a time $\tau = t - T_{21}$ following the readout pulse is given by

$$S(T_{21}, \tau) = e^{-\Gamma_c T_{21}}e^{-\Gamma_b\tau_r}J^2\Theta(\tau_r)|C(T_{21})|^2, \tag{59}$$

where

$$J = \frac{\mu_{ba}\mathcal{N}L}{4}\left(\frac{\omega_{ba}^2}{4\pi\epsilon_0 c^2}\right)\int d\boldsymbol{\rho}\, \sin[A_e(\boldsymbol{\rho})]\sin[A_{\rm out}(\boldsymbol{\rho})], \tag{60}$$

$$\tau_r = \tau - \frac{R_d}{c} = t - T_{21} - \frac{R_d}{c}, \tag{61}$$

Θ is a Heaviside function, and

$$\begin{aligned} C(T_{21}) &= \mathrm{Tr}\left[U_{ba}(k_1\mathbf{u}_x, T_{21})^\dagger\rho_{ba}^I(T_{21}^+)\right] \\ &= \mathrm{Tr}\left[\begin{matrix} U_{ba}(k_1\mathbf{u}_x, T_{21})^\dagger U_{cb}(-k_2\mathbf{u}_x, T_{21})^\dagger \\ \times U_{ca}[k_{12}\mathbf{u}_x, 0]\rho_{aa}(0)\end{matrix}\right] \\ &= \mathrm{Tr}[U_{ca}(k_{12}\mathbf{u}_x, T_{21})^\dagger U_{ca}(k_{12}\mathbf{u}_x, 0)\rho_{aa}(0)] \\ &= \sum_{q,q',q''} e^{-i\omega_{cq';aq}T_{21}}B_{aq;cq'}^\dagger(k_{12}\mathbf{u}_x) \\ &\quad \times B_{cq';aq''}(k_{12}\mathbf{u}_x)\rho_{q''q}(0). \end{aligned} \tag{62}$$

The matrices B and $B^\dagger$ are defined in Eqs. (8). The matrix $U_{ba}(\mathbf{k}_{ba}, t_r)^\dagger$ appearing in Eq. (44) has been evaluated at

$t_r = T_{21}$, based on the assumptions that the atomic center-of-mass motion is frozen during the readout pulse and that $|\omega_{bq;aq'}|R_d/c \ll 1$. Note that state b has dropped out of the calculation. Equation (62) can be evaluated for various trap potentials.

It has been assumed that the trap potential is constant over the excitation volume and that any transverse motion can be neglected on a timescale equal to T_{21}. As a consequence, a normalized signal can be defined by

$$\tilde{S}(T_{21}) = \frac{S(T_{21},\tau)}{S(0,\tau)} = e^{-\Gamma_c T_{21}}|C(T_{21})|^2 \tag{63}$$

that depends only on T_{21} and the nature of the lattice potentials. In other words, $\tilde{S}(T_{21})$ does not depend on the spatial profiles of the excitation and readout pulses. Thus, it is not necessary to specify the excitation and readout fields in the graphs of $|C(T_{21})|^2$ that are be presented in this section.

A. State-independent potentials

In general, Eq. (62) must be used to calculate $C(T_{21})$, with matrix elements given by Eqs. (8). However, for *state-independent* potentials, the *internal* state does not have to be specified in calculating the matrix elements. In that case,

$$C(T_{21}) = \sum_{q,q'}\langle q|e^{iH_aT_{21}/\hbar}e^{-ik_{12}X}e^{-iH_cT_{21}/\hbar}e^{ik_{12}X}|q'\rangle \times \rho_{q'q}(0) = \langle e^{-ik_{12}\hat{X}(T_{21})}e^{ik_{12}\hat{X}(0)}\rangle, \tag{64}$$

where $\hat{X}(T_s)$ and $\hat{X}(0)$ are Heisenberg operators. Of course, Eq. (64) is all but impossible to evaluate except for free atoms or for atoms moving in a harmonic potential. For our specific choice of potentials, we have

$$V_a(X) = V_c(X) = V(X) = -V_0 + V_0\sin^2(k_{tr}X), \tag{65}$$

with

$$V_0 = \frac{1}{2}\frac{M\omega^2}{k_{tr}^2}. \tag{66}$$

1. Harmonic potential

In the harmonic approximation, that is, when the level a and c potentials are replaced by

$$V(X) \sim -V_0 + \tfrac{1}{2}M\omega^2X^2, \tag{67}$$

it is possible to evaluate Eq. (64) directly, without reverting to Eq. (62). For Eq. (67) to be a good approximation, a necessary condition is

$$\frac{V_0}{\hbar\omega} = \frac{1}{2}\frac{M\omega^2}{\hbar\omega k_{tr}^2} = \frac{1}{4\zeta_{tr}^2} \gg 1, \tag{68}$$

where

$$\zeta_{tr} = k_{tr}\sqrt{\frac{\hbar}{2M\omega}} \tag{69}$$

is the trap-field Lamb-Dicke parameter.

In the harmonic approximation

$$k_{12}\hat{X}(T_{21}) = k_{12}\left[\hat{X}(0)\cos(\omega T_{21}) + \frac{\hat{P}(0)}{M\omega}\sin(\omega T_{21})\right] = \zeta[ae^{-i\omega T_{21}} + a^\dagger e^{i\omega T_{21}}], \tag{70}$$

where

$$\zeta = k_{12}\sqrt{\frac{\hbar}{2M\omega}} \tag{71}$$

is the effective Lamb-Dicke parameter for the excitation field,

$$a = \frac{\hat{\xi}+i\hat{v}}{\sqrt{2}}, \tag{72a}$$

$$a^\dagger = \frac{\hat{\xi}-i\hat{v}}{\sqrt{2}}, \tag{72b}$$

$$\hat{\xi} = \sqrt{\frac{M\omega}{\hbar}}\hat{X}(0), \tag{73a}$$

$$\hat{v} = \frac{1}{\sqrt{\hbar M\omega}}\hat{P}(0), \tag{73b}$$

such that

$$C(T_{21}) = \left\langle e^{-i\zeta[ae^{-i\omega T_{21}}+a^\dagger e^{i\omega T_{21}}]}e^{i\zeta[a+a^\dagger]}\right\rangle = e^{-i\zeta^2\sin(\omega T_{21})}\left\langle e^{\sigma(T_{21})a^\dagger-\sigma(T_{21})^*a}\right\rangle \tag{74}$$

with

$$\sigma(T_{21}) = i\zeta[1-e^{i\omega T_{21}}]. \tag{75}$$

The evaluation of the characteristic function

$$\left\langle e^{\sigma(T_{21})a^\dagger-\sigma(T_{21})^*a}\right\rangle$$

for various initial states can be found in standard texts [26].

a. Coherent state. For atoms prepared in a coherent state $|\alpha\rangle$,

$$C(T_{21}) = e^{-i\zeta^2\sin(\omega T_{21})}e^{-|\sigma(T_{21})|^2/2}e^{\sigma(T_{21})\alpha^*-\sigma(T_{21})^*\alpha} \tag{76}$$

and

$$|C(T_{21})| = e^{-|\sigma(T_{21})|^2/2}, \tag{77}$$

with

$$|\sigma(T_{21})|^2 = 2\zeta^2[1-\cos(\omega T_{21})]. \tag{78}$$

There is minimal dephasing for a small Lamb-Dicke parameter. This dephasing is a pure quantum effect, which vanishes in the limit that $\hbar \to 0$. In the analogous classical problem, $|C(T_{21})| = 1$ since all atoms have the same initial conditions.

b. Density matrix diagonal in number basis. If the atoms are prepared in a state having a density matrix that is diagonal in the number representation

$$\rho_{nn'}(0) = P_n\delta_{n,n'}, \tag{79}$$

then [26]

$$C(T_{21}) = e^{-i\zeta^2\sin(\omega T_{21})}e^{-|\sigma(T_{21})|^2/2}\sum_{n=0}^{\infty}P_nL_n(|\sigma(T_{21})|^2), \tag{80}$$

where $L_n(z)$ is a Laguerre polynomial.

For atoms prepared in a number state $P_q = \delta_{q,n}$,

$$|C(T_{21})| = e^{-|\sigma(T_{21})|^2/2}L_n(|\sigma(T_{21})|^2). \tag{81}$$

The value of $C(T_{21})$ is identical for an initial coherent state and an initial vacuum state since the spatial widths of both packets are identical and do not change in time.

For a thermal state with

$$P_n = (1-e^{-\beta})e^{-n\beta}, \quad \beta = \frac{\hbar\omega}{k_B T}, \tag{82}$$

$$|C(T_{21})| = e^{-|\sigma(T_{21})|^2/2}(1-e^{-\beta})\sum_{n=0}^{\infty} e^{-n\beta} L_n(|\sigma(T_{21})|^2)$$
$$= e^{-\frac{1}{2}|\sigma(T_{21})|^2\coth(\beta/2)} = e^{-\zeta^2[1-\cos(\omega T_{21})]\coth(\beta/2)}. \tag{83}$$

For a Poissonian distribution,

$$P_n = e^{-\bar{n}}\frac{\bar{n}^n}{n!}, \tag{84}$$

$$|C(T_{21})| = e^{-|\sigma(T_{21})|^2/2}e^{-\bar{n}}\sum_{n=0}^{\infty}\frac{\bar{n}^n}{n!}L_n(|\sigma(T_{21})|^2), \tag{85}$$

which must be evaluated numerically. For large $\bar{n}$, the result is similar to the result for a number state having $n = \bar{n}$.

c. Squeezed vacuum. For a squeezed vacuum with squeeze parameter $z = re^{i\theta}$ [26],

$$|C(T_{21})| = |\langle 0|e^{g(T_{21})a^\dagger - g(T_{21})^* a}|0\rangle| = e^{-|g(T_{21})|^2/2}, \tag{86}$$

where

$$g(T_{21}) = \sigma(T_{21})\cosh r + \sigma^*(T_{21})e^{i\theta}\sinh r. \tag{87}$$

For a squeezing parameter $r \gg 1$, $|C(T_{21})| \ll 1$, in general. Of course, $C(T_{21}) = 1$ at the revival times when ωT_{21} is an integral multiple of 2π. However, there is an *additional* time during each period when there is a complete revival, occurring when $\omega T_{21} = \theta \pm (2n+1)\pi$. For example, when θ equals zero, additional revivals occur for values ωT_{21} that are odd integral multiples of π. In this case, from Eq. (70),

$$k_{12}[\hat{X}(T_{21} = \pi/\omega)] = -k_{12}\hat{X}(0). \tag{88}$$

Since the momentum operator no longer appears, the signal can be optimized by squeezing the spatial distribution. For values $\omega T_{21} = \theta \pm (2n+1)\pi$, it is some combination of the momentum and coordinate distributions that is squeezed.

In Fig. 2, we plot $|C(T_{21})|^2$ as a function of ωT_{21} for initial pure number-state and Poissonian distributions, with $\zeta = 0.23$. It is seen that if $\bar{n}$ of the Poissonian distribution equals n of the number-state distribution, the two results do not differ by much. In Fig. 3, we plot $|C(T_{21})|^2$ as a function of ωT_{21} for initial coherent state (solid red curve) and squeezed vacuum state distributions (dashed blue and solid black curves), with $\zeta = 0.23$. The dashed blue curve is for squeezing parameters $r = 1.5$, $\theta = 0$ and the solid black for $r = 4$, $\theta = 0$. The extra peaks at $\omega T_{21} = (2n+1)\pi$ are a clear signature of the quantum nature of the initial motional state associated with the squeezed vacuum.

d. Classical limit. We can take a classical limit of Eq. (64) by ignoring the commutator of $\hat{X}(T_s)$ and $\hat{X}(0)$ and replacing the operators by their classical counterparts to arrive at

$$C_{cl}(T_{21}) \sim \left\langle e^{-ik_{12}[X(T_{21})-X(0)]}\right\rangle$$
$$= \left\langle e^{-ik_{12}[X_0[\cos(\omega T_{21})-1]+(v_0/\omega)\sin(\omega T_{21})]}\right\rangle, \tag{89}$$

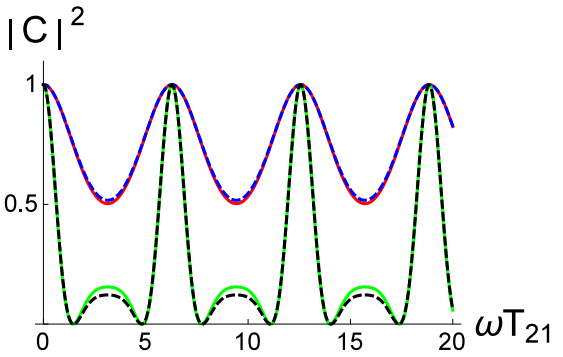

FIG. 2. Plots of $|C(T_{21})|^2$ as a function of ωT_{21} for a state-independent, harmonic lattice potential and for initial number state and Poissonian distributions, with $\zeta = 0.23$. The (upper) solid red and (lower) green curves are for initial number-state distributions with $n = 1$ and 15, respectively. The dashed upper blue and lower black curves are for initial Poissonian distributions with $\bar{n} = 1$ and 15, respectively.

where the average is now a classical average over the distribution of initial conditions. For a thermal distribution,

$$W_0(X_0, v_0) = \frac{M\omega}{2\pi k_B T}\exp\left[-\frac{1}{2}\frac{Mv_0^2 + M\omega^2 X_0^2}{k_B T}\right], \tag{90}$$

we find

$$|C_{cl}(T_{21})| = e^{-2\zeta^2[1-\cos(\omega T_{21})]/\beta}$$
$$= \exp\left[-\frac{k_B T}{2V_0}\frac{k_{12}^2}{k_{tr}^2}[1-\cos(\omega T_{21})]\right], \tag{91}$$

independent of $\hbar$. The classical [Eq. (91)] and quantum [Eq. (83)] results agree for $\beta \ll 1$ (high-temperature limit). Somewhat remarkably, even for $\beta = 1$, the difference between the classical and quantum predictions is small if the Lamb-Dicke parameter is less than or of order unity. For $\beta \gg 1$ (low-temperature limit), $|C_{cl}(T_{21})| \sim 1$, whereas $|C(T_{21})| \sim e^{-\frac{1}{2}|\sigma(T_{21})|^2}$. A comparison of the classical and quantum results is shown in Fig. 4, with $\zeta = 0.23$. The solid curves are the quantum results and the dashed curves the classical results. It is seen that, even for $\beta = 0.5$, the two results practically

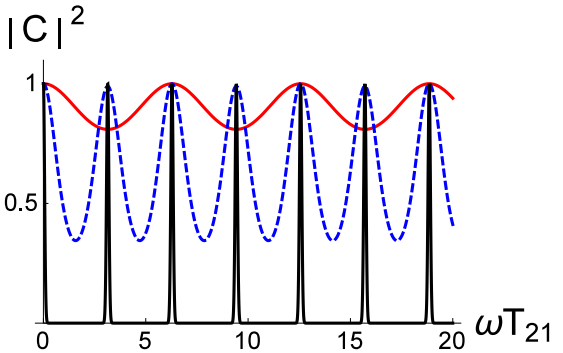

FIG. 3. Plots of $|C(T_{21})|^2$ as a function of ωT_{21} for a state-independent, harmonic lattice potential and for initial coherent state (solid upper red curve) and squeezed vacuum state distributions (dashed blue curve $r = 1.5$, solid lower black curve $r = 4$), with $\zeta = 0.23$.

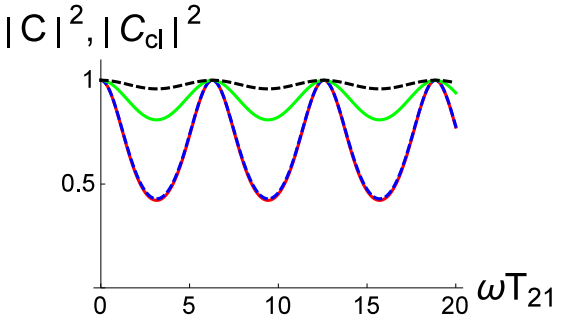

FIG. 4. Plots of $|C(T_{21})|^2$ and $|C_{cl}(T_{21})|^2$ as a function of ωT_{21} for a state-independent, harmonic lattice potential and for initial thermal distributions, with $\zeta = 0.23$. The solid lower red and upper green curves are the quantum results with $\beta = 0.5$ and 10, respectively. The dashed lower blue and upper black curves are the corresponding classical results.

overlap. On the other hand, for very cold atoms, $\beta = 10$, the classical result is almost equal to unity, whereas the quantum result still exhibits dephasing owing to the spread of momentum in the ground-state wave function.

2. Anharmonic motion

If the potential is not sufficiently deep for the harmonic approximation to be valid, it is necessary to use the eigenfunctions and eigenenergies for a potential that varies as $V_0 \sin^2(k_{tr}X_0)$ (the $-V_0$ part of the potential can be dropped since it plays no role in this calculation). The periodic eigenfunctions and eigenvalues for a $\sin^2(k_{tr}X_0)$ potential are the so-called A_n and B_{n+1} Mathieu functions [27]. As long as the potential is sufficiently deep and the temperature sufficiently low, the only eigenfunctions of importance are those associated with the quasibound states of the potentials for which the A_n and B_{n+1} Mathieu functions are nearly identical, as are the eigenenergies associated with these eigenfunctions. This is the only limit we will consider.

The calculation of Eq. (62) must now be carried out numerically. For $\zeta = 0.23$ and $\zeta_{tr} = 0.16$, results are shown in Figs. 5 and 6 as the solid red curves for $\beta = 0.41$ and

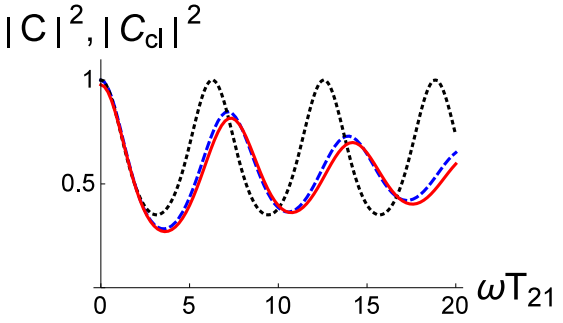

FIG. 5. Plots of $|C(T_{21})|^2$ and $|C_{cl}(T_{21})|^2$ as a function of ωT_{21} for a state-independent, anharmonic lattice potential and for an initial thermal distribution with $\zeta = 0.23$, $\zeta_{tr} = 0.16$, and $\beta = 0.41$. The solid red curve is the quantum result, the dashed blue curve is the classical result, and the dotted black curve is the quantum result for the corresponding harmonic potential.

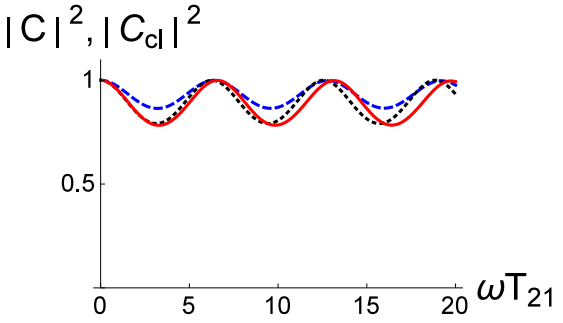

FIG. 6. Same as Fig. 5, but with $\beta = 3$.

$\beta = 3$, respectively. The integrals of the type given in Eq. (58) are restricted to a single well using appropriately normalized Mathieu functions. The anharmonicity leads to a reduction of the amplitude of oscillation, as well as a decay of the signal, owing to the continuous range of frequencies present in the response. For comparison, the results for the corresponding harmonic potential are shown as the dotted black curves in the figures. Even in the case of cold atoms, $\beta = 3$, when the harmonic approximation is expected to be good, the anharmonic and harmonic results begin to diverge at longer times, owing to the fact that small changes in frequency can still lead to significant phase shifts for sufficiently long times.

Classical limit. The fact that the classical and quantum results for a harmonic potential are nearly identical for $\beta \lesssim 1$ when $\zeta < 1$ suggests that the quantum and classical results for a potential that varies as $V_0 \sin^2(k_{tr}X)$ might also be nearly identical. The total energy associated with the center-of-mass motion of an atom can be written as

$$E = \frac{1}{2}\left[M\left(\frac{dX}{dt}\right)^2 + \frac{M\omega^2}{k_{tr}^2}\sin^2(k_{tr}X)\right], \tag{92}$$

where ω is defined by Eq. (66), and X and dX/dt are the position and velocity of the atom. Setting $k_{tr}X = z$ and $\omega t = \tau$, and using Eqs. (71) and (82), we can rewrite the energy as

$$E = \frac{\beta k_B T}{4\zeta_{tr}^2}(\dot{z}^2 + \sin^2 z), \tag{93}$$

where the dot signifies differentiation with respect to τ.

The equation of motion for an atom moving in this potential is

$$\ddot{z} = -\frac{\sin z}{2}. \tag{94}$$

The solution of this equation can be written as

$$z(\tau) = \text{JacobiAmplitude}\left[\begin{matrix}\text{EllipticFunctionF}\left(z_0; \frac{1}{\epsilon}\right) \\ +\sqrt{\epsilon}\tau, \frac{1}{\epsilon}\end{matrix}\right], \tag{95}$$

where

$$\epsilon = \left(\dot{z}_0^2 + \sin^2 z_0\right), \tag{96}$$

$z_0 = z(0)$, and $\dot{z}_0 = \dot{z}(0)$, and JacobiAmplitude and EllipticFunctionF are built-in functions in *Mathematica*. It then follows that, for a thermal distribution with E given by

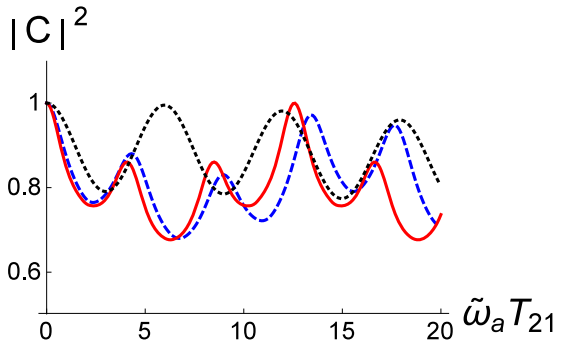

FIG. 7. Graphs of $|C(T_{21})|^2$ as a function of $\tilde{\omega}_a T_{21}$ for a state-dependent, harmonic lattice potential and for a thermal initial state with $\zeta = 0.23$, $\beta = 3$, and $s = 1.05$ (black, dotted curve), $s = \sqrt{2}$ (blue, dashed curve), and $s = 1.5$ (red, solid curve).

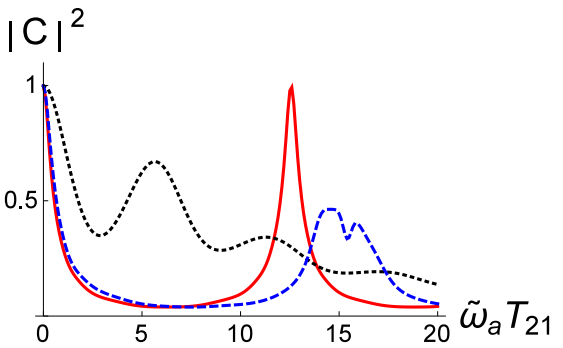

FIG. 8. Graphs of $|C(T_{21})|^2$ as a function of $\tilde{\omega}_a T_{21}$ for a state-dependent, harmonic lattice potential and for a thermal initial state with $\zeta = 0.23$, $\beta = 0.41$, and $s = 1.05$ (black, dotted curve), $s = \sqrt{2}$ (blue, dashed curve), and $s = 1.5$ (red, solid curve).

Eq. (93),

$$|C_{cl}(T_{21})|^2 = \frac{\int_{-\pi/2}^{\pi/2} dz_0 \int_{-\sqrt{1-\sin^2 z_0}}^{\sqrt{1-\sin^2 z_0}} d\dot{z}_0 e^{-\frac{\beta}{4\zeta_{tr}^2}(\dot{z}_0^2+\sin^2 z_0)-i[z(\omega T_{21})-z_0]}}{\int_{-\pi/2}^{\pi/2} dz_0 \int_{-\sqrt{1-\sin^2 z_0}}^{\sqrt{1-\sin^2 z_0}} d\dot{z}_0 e^{-\frac{\beta}{4\zeta_{tr}^2}(\dot{z}_0^2+\sin^2 z_0)}}, \tag{97}$$

where the integrals have been restricted to bound-state motion. The integrals can be evaluated numerically. In Figs. 5 and 6, $|C_{cl}(T_{21})|^2$ is plotted as the dashed blue curves for $\beta = 0.41$ and 3, respectively. As can be seen, the classical and quantum results are in good agreement for $\beta = 0.41$, but differ somewhat for cold atoms, $\beta = 3$, when the classical picture is expected to fail.

B. State-dependent potentials

When the potentials are state dependent, it is necessary to revert to Eq. (62). We could consider both harmonic and anharmonic potentials. However, both anharmonicity and state dependence produce dephasing that can be attributed to more than one frequency in the problem. By limiting the discussion to harmonic potentials, we can isolate the contribution of the state dependence to this dephasing. In the harmonic limit, Eq. (47) for the potentials reduces to

$$V_\alpha(\mathbf{R}) \approx -V_\alpha + \tfrac{1}{2} M \tilde{\omega}_\alpha^2 X^2, \quad \alpha = a, c. \tag{98}$$

From Eq. (62), it is seen that, for incommensurable frequencies $\tilde{\omega}_a$ and $\tilde{\omega}_c$ of the motional states of the level a and c potentials defined in Eq. (48), there are no complete revivals of the signal. On the other hand, if $\tilde{\omega}_c = (m/n)\tilde{\omega}_a$, where both m and n are integers and n is the least common denominator, then revivals occur at integral multiples of $\tilde{\omega}_a T_{21} = 2n\pi$. In Figs. 7 and 8, we plot $|C(T_{21})|^2$ as a function of $\tilde{\omega}_a T_{21}$ for a thermal initial state with $\zeta = 0.23$, $\beta = 3$ or 0.41, and several values of $s = \tilde{\omega}_c/\tilde{\omega}_a$.

For cold atoms, $\beta = 3$, most of the initial population is in the ground state and only the frequencies associated with the lowest transitions in both wells appear in the signal (Fig. 7). For $s = 1.05$, these frequencies are not resolved and we see a slight damping of the signal. For $s = 1.5$ and $\sqrt{2}$, both frequencies are evident, as is the complete revival of the signal at $\tilde{\omega}_a T_{21} = 4\pi$ for $s = 1.5$. For $s = 1.05$ there is a complete revival (not shown) at $\tilde{\omega}_a T_{21} = 40\pi$.

The situation changes for hotter atoms, $\beta = 0.41$, since many transitions contribute to the signal and tend to wash out the signal, as shown in Fig. 8. For $s = 1.05$, the signal is damped, a complete revival would occur at $\tilde{\omega}_a T_{21} = 40\pi$. For $s = 1.5$, the complete revival is seen at $\tilde{\omega}_a T_{21} = 4\pi$. Somewhat surprisingly, there is a *partial* revival for incommensurate frequencies, $s = \sqrt{2}$. It is not difficult to understand why this occurs. If we write $s = 1 + \sigma$ and insert this into Eq. (62), we see that, for times $\tilde{\omega}_a T_{21} = 2n\pi/\sigma$, the expression reduces to that for a *state-independent harmonic potential* having frequency $\tilde{\omega}_a$. The value of $|C(T_{21})|^2$ for a state-independent potential is calculated using Eq. (83) as $\exp\{-2\zeta^2[1 - \cos(\tilde{\omega}_a T_{21})]\coth(\beta/2)\}$. For $\beta = 0.41$ and $\zeta = 0.23$, $|C(T_{21})|^2 \geqslant 0.35$ so a partial revival is seen at integral multiples of $\tilde{\omega}_a T_{21} = 2\pi/\sigma$.

An additional effect enters the calculation that is not present for state-independent potentials. Owing to the difference in the values of V_α the energy levels in the harmonic potentials are displaced by different amounts. In other words, we have assumed in Eq. (98) that both $\tilde{\omega}_\alpha$ and V_α are independent of the transverse coordinate $\boldsymbol{\rho}$. If this assumption is not valid for V_α, $C(T_{21})$ must be multiplied by an additional factor $\exp\{-i[V_c(\boldsymbol{\rho}) - V_a(\boldsymbol{\rho})]T_{21}/\hbar\}$ and included in the average over the excitation field spatial profiles. This would result in a damping of the signal with increasing T_{21}, making it difficult to observe the revivals when the potentials differ significantly.

V. SPECIFIC EXAMPLE: RAMAN COHERENCE–TRANSIT-TIME EFFECTS

We now turn our attention to the level scheme of Fig. 1(b) and assume copropagating excitation fields with $k_1 \approx k_2$. In this limit we can ignore the spatial phase factors in Eqs. (8). We still assume that the trap potential is constant over the excitation volume but no longer neglect the transverse motion of the atoms. As such, the only net effect that we study in this section is one of *transit-time* loss and revival. The excitation fields carve out an excitation volume, but atomic motion takes atoms out of this volume, an effect that is monitored by the readout pulse. In essence, this is a quantum

treatment of transit-time effects, which can be compared with the classical results for free atoms [28] or atoms in traps. We consider only harmonic traps and state-independent, harmonic potentials having characteristic frequency ω. It is not much more difficult to generalize the results to state-dependent potentials, but they have little effect on the transit-time effects under investigation in the section. Their only effect would be to degrade the periodic revivals of the emitted signal that would occur for harmonic traps at half-integral multiples of the trap period. The readout field and two fields comprising the excitation field are assumed to have the same waist w_e.

A. Classical limit

We consider first the classical limit, for which the normalized signal can be written as

$$\tilde{S}(T_{21}) = \frac{S(T_{21},\tau)}{S(0,\tau)} = \tilde{S}_{cl}(T_{21}), \tag{99}$$

where

$$\tilde{S}_{cl}(T_{21}) = \left|\frac{C_{cl}(T_{21})}{C_{cl}(0)}\right|^2, \tag{100}$$

$$C_{cl}(T_{21}) = \tfrac{1}{4}\left\langle \sin\left[A_e e^{-2\rho(0)^2/w_e^2}\right]\sin\left[A_{\rm out}e^{-\rho(T_{21})^2/w_e^2}\right]\right\rangle, \tag{101}$$

$$\boldsymbol{\rho}(0) = \boldsymbol{\rho}_0, \tag{102a}$$

$$\boldsymbol{\rho}(t) = \boldsymbol{\rho}_0\cos(\omega t) + \frac{\mathbf{v}_0}{\omega}\sin(\omega t), \tag{102b}$$

and the average is taken with the classical Maxwell-Boltzmann distribution given in Eq. (90). We can no longer write the normalized signal $\tilde{S}(T_{21})$ as a function of $C(T_{21})$ alone since the transverse spatial profiles of the excitation and readout fields no longer factor out of the expression for the signal when the transverse motion of the atoms is included (in the calculation involving the optical lattice, the transverse motion was neglected). With a change of variables to dimensionless coordinates, we can wite Eq. (101) as

$$C_{cl}(T_{21}) = \frac{1}{16\pi^2}\int_{-\infty}^{\infty}dy\int_{-\infty}^{\infty}dv_y\int_{-\infty}^{\infty}dz\int_{-\infty}^{\infty}dv_z e^{-(y^2+v_y^2)/2}e^{-(z^2+v_z^2)/2}\sin\left(A_e e^{-\kappa^2(y^2+z^2)}\right)$$
$$\times\ \sin\left(A_{\rm out}\exp\left\{-\frac{\kappa^2}{2}\left[(y^2+z^2)\cos^2(\omega T_{21}) + (v_y^2+v_z^2)\sin^2(\omega T_{21}) + (yv_y+zv_z)\sin(2\omega T_{21})\right]\right\}\right), \tag{103}$$

where

$$\kappa = \sqrt{\frac{2k_BT}{M\omega^2 w_e^2}} = \frac{w_{th}}{w_e}, \tag{104}$$

and

$$w_{th} = \sqrt{\frac{2k_BT}{M\omega^2}} \tag{105}$$

is the spatial width associated with the classical Boltzmann distribution at temperature T.

If the sin functions are expanded, all the integrals can be evaluated analytically and the result expressed as

$$C_{cl}(T_{21}) = \frac{1}{4}\sum_{n,m=0}^{\infty}\frac{(-1)^{n+m}A_e^{(2n+1)}A_{\rm out}^{(2m+1)}}{(2n+1)!(2m+1)!}\,\frac{1}{1+\kappa^2(3+2m+4n)+2\kappa^4(2n+1)(2m+1)\sin^2(\omega T_{21})}. \tag{106}$$

In the perturbation theory limit $A_e, A_{\rm out} \ll 1$,

$$C_{cl}(T_{21}) \sim \frac{A_eA_{\rm out}/4}{1+3\kappa^2+2\kappa^4\sin^2(\omega T_{21})} \tag{107}$$

and

$$\tilde{S}_{cl}(T_{21}) \sim \left[1+\frac{2\kappa^4\sin^2(\omega T_{21})}{1+3\kappa^2}\right]^{-2}. \tag{108}$$

In Fig. 9, $\tilde{S}_{cl}(T_{21})$ is plotted as a function of ωT_{21} for $\beta = 0.1$, $\kappa = 1, 5$ and $(A_1, A_2) = (0.1, 0.1)$, $(\pi/2, \pi/2)$. The signal decays owing to transit-time effects, but eventually revives for $\omega T_{21} = n\pi$; that is, any atoms that leave the excitation volume return to it after each half-period of oscillation. There is not much difference in the *normalized* signal for weak pulses and (optimal) $\pi/2$ pulses. The transit-time regime is shown in Fig. 10 for $\kappa = 3, 8$ and $(A_1, A_2) = (0.1, 0.1)$, $(\pi/2, \pi/2)$.

To a good approximation, the weak-field result for $\kappa^2 \gg 1$ and $\omega T_{21} \ll 1$ is the square of a Lorentzian,

$$\tilde{S}_{cl}(T_{21}) \sim \frac{1}{\left[1+\frac{2\kappa^2(\omega T_{21})^2}{3}\right]^2}, \tag{109}$$

having half-width

$$\omega T_{21} = \frac{\sqrt{3(\sqrt{2}-1)/2}}{\kappa}. \tag{110}$$

The classical results can be given a simple interpretation. In this picture involving classical center-of-mass motion, any atom j that is in the initial excitation volume has a coherence $\rho_{ac}^{(j)}$ created by the excitation field. When probed by the readout field, atom j will contribute to the phase-matched signal, provided it is *still* in the excitation volume at the time of the readout pulse. The time it takes an atom to leave the

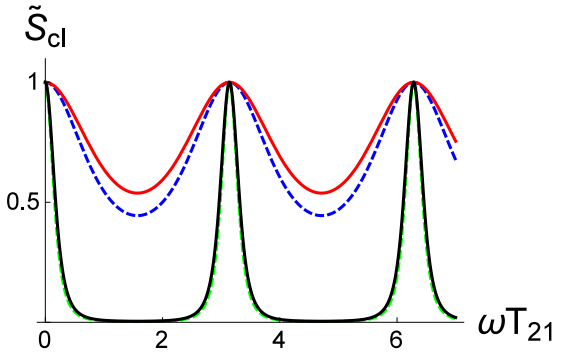

FIG. 9. Plots of $\tilde{S}_{cl}(T_{21})$ as a function of ωT_{21} for a state-independent, transverse harmonic potential and for initial thermal distributions, with $\beta = 0.1$ and $\kappa = 1$ (upper red and blue curves); $\kappa = 5$ (lower black and green curves). The solid curves are for pulse areas $(A_1, A_2) = (0.1, 0.1)$ and the dashed curves for $(A_1, A_2) = (\pi/2, \pi/2)$.

excitation volume is of order $t_{cl} = w_e/u_{th}$, where

$$u_{th} = \sqrt{\frac{2k_B T}{M}} \tag{111}$$

is the velocity width associated with the classical Boltzmann distribution at temperature T. Therefore, we would expect a transit-time width of order

$$\omega t_{cl} = \omega w_e/u_{th} = 1/\kappa, \tag{112}$$

which is what we found. Of course, at half-integral multiples of the trap period, any atom that was excited initially is back in the excitation volume.

The quantity w_{th} is the width of the Boltzmann distribution. For $\kappa^2 \ll 1$, the excitation field width w_e is much larger than w_{th}; as a consequence, almost *all* the atoms are excited by the field. The Maxwellian velocity distribution results in some loss of population from the excitation volume as time progresses, but this is a minimal loss since very few atoms move outside this large excitation volume in a trap period, implying that $\tilde{S}_{cl}(T_{21}) \sim 1$. For $1 < \kappa^2 \ll 10$, about a half

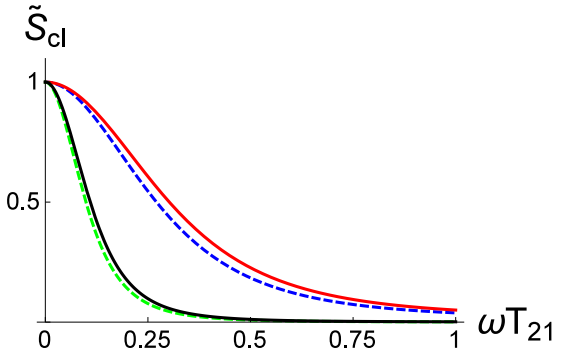

FIG. 10. Plots of $\tilde{S}_{cl}(T_{21})$ illustrating transit-time decay as a function of ωT_{21} for a state-independent, transverse harmonic potential and for initial thermal distributions, with $\beta = 0.1$ and $\kappa = 3$ (upper red and blue curves); $\kappa = 8$ (lower black and green curves). The solid curves are for pulse areas $(A_1, A_2) = (0.1, 0.1)$ and the dashed curves for $(A_1, A_2) = (\pi/2, \pi/2)$.

to a quarter of the atoms are excited by the first pulse. The velocity distribution of the chosen atoms is still given by the initial Maxwellian distribution since there is no velocity selection in the excitation process. Between the revival times a significant percentage of this population migrates out of the excitation region, leading to a signal loss that depends on T_{21}. For $\kappa^2 \gg 10$ only a very small fraction of the atoms are excited and they quickly migrate out of the excitation volume. The signal in this case is a series of spikes of unit amplitude at the revival times, with virtually no signal between those times.

B. Quantum calculation

We want to derive the corresponding results for a quantum thermal distribution. We expect that a quantum description is needed if either of two conditions are not met. First, when $\beta \gg 1$, most of the initial-state population is in the quantum ground state, which introduces quantum corrections. That is, the quantum and classical results will differ whenever $\beta \gg 1$, even though these differences may be small in an absolute sense if $\kappa \ll 1$. The second condition can be inferred from Eq. (83), where, even for $\beta \ll 1$, there are quantum corrections of order $\beta\zeta^2$. In the transit-time calculation, ζ is replaced by $\zeta_e = \sqrt{\hbar/2M\omega w_e^2}$ and

$$\beta\zeta^2 \to \beta\zeta_e^2 = \beta^2\kappa^2/4. \tag{113}$$

Thus, we can expect quantum corrections to contribute when $\beta\kappa > 1$, even if $\beta \ll 1$. This is related to the fact that the narrow spatial distribution that is excited when $\kappa \gg 1$ can lead to uncertainties in the momentum distribution (owing to the uncertainty principle) that are larger than those already present in the thermal momentum distribution.

Since the *normalized* signal does not depend strongly on the pulse areas, it suffices to calculate $S(T_{21})$ in the quantum case assuming pulse areas much less than unity. The normalized signal, written using dimensionless coordinates, factors into equal contributions from each of the transverse coordinates. As a consequence, we can write

$$\tilde{S}(T_{21}) = \left|\frac{C(T_{21})}{C(0)}\right|^4, \tag{114}$$

where

$$C(T_{21}) = \sum_{q,q',q''=0}^{\infty} e^{-i\omega_{cq';aq}T_{21}} \langle q|e^{-\beta\kappa^2\xi^2}|q'\rangle \times \langle q'|e^{-\beta\kappa^2\xi^2/2}|q''\rangle \rho_{aq'';aq}(0), \tag{115}$$

ξ is a dimensionless coordinate, and the q's are quantum numbers of a one-dimensional oscillator potential. Transit-time effects enter implicitly through the exponential time factors in Eq. (115). The needed matrix elements can be evaluated explicitly using

$$\langle q|e^{-g^2\xi^2}|q'\rangle = \frac{(-2g^2)^{\frac{q+q'}{2}}\Gamma\left(\frac{1+q+q'}{2}\right)}{\sqrt{\pi q!q'!}(1+g^2)^{\frac{1+q+q'}{2}}} \times {}_2F_1\left(-q, -q', \frac{1-q-q'}{2}, \frac{1+g^2}{2g^2}\right), \tag{116}$$

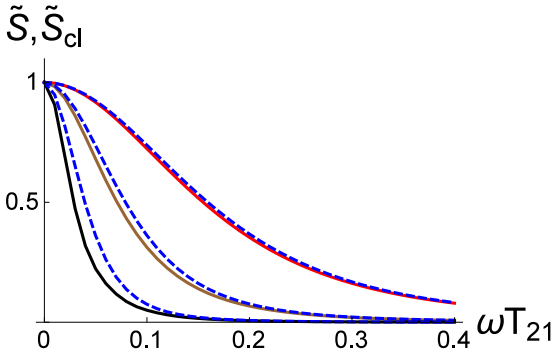

FIG. 11. Plots of $\tilde{S}_{cl}(T_{21})$ and $\tilde{S}_{cl}(T_{21})$ as a function of ωT_{21} for a state-independent, transverse harmonic potential, perturbative excitation and readout pulses, and for initial thermal distributions, for $\beta = 0.1$ and $\kappa = 5$ (upper solid red curve); $\kappa = 10$ (middle solid brown curve), and $\kappa = 20$ (lower solid black curve). The dashed blue curves are the classical results for the same parameters.

where Γ is the gamma function and ${}_2F_1$ is a hypergeometric function.

If the initial density matrix is diagonal,

$$\rho_{qq'}(0) = P_q \delta_{q,q'}, \tag{117}$$

then

$$C(T_{21}) = \sum_{q,q'=0}^{\infty} P_q e^{-i(q'-q)\omega T_{21}} \langle q|e^{-\beta\kappa^2\xi^2}|q'\rangle\langle q'|e^{-\beta\kappa^2\xi^2/2}|q\rangle. \tag{118}$$

For a thermal state with $P_q = (1 - e^{-\beta})e^{-q\beta}$ ($\beta = \hbar\omega/k_B T$), Eq. (118) is evaluated numerically using Eq. (116) for different values of β and κ^2.

In Fig. 11, $\tilde{S}(T_{21})$ is plotted as a function of ωT_{21} for $\beta = 0.1$ and $\kappa = 5$; ($\beta\kappa = 0.5$), $\kappa = 10$; ($\beta\kappa = 1$), and $\kappa = 20$ ($\beta\kappa = 2$), along with the classical result $\tilde{S}_{cl}(T_{21})$. With increasing values of $\beta\kappa$, the classical and quantum results begin to deviate. In Fig. 12, $\tilde{S}(T_{21})$ is plotted as a function of ωT_{21} for $\kappa = 1$ and $\beta = 1, 5, 10$, along with the classical result

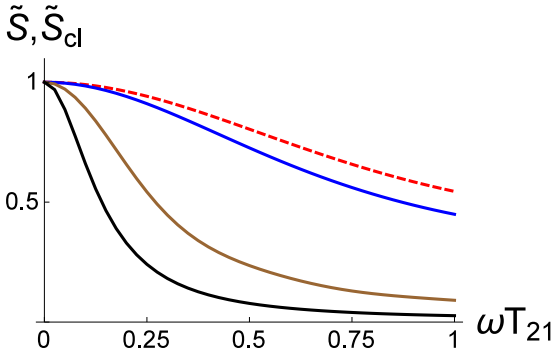

FIG. 12. Plots of $\tilde{S}_{cl}(T_{21})$ and $\tilde{S}_{cl}(T_{21})$ as a function of ωT_{21} for a state-independent, transverse harmonic potential, perturbative excitation and readout pulses, and for initial thermal distributions for $\kappa = 1$ and $\beta = 1$ (upper solid blue curve); $\beta = 5$ (middle brown curve), and $\beta = 10$ (lower black curve). The dashed red curve is the classical result which is the same for all β if κ is held fixed.

$\tilde{S}_{cl}(T_{21})$. With increasing β, the signal deviates significantly from the classical result.

We can estimate the signal for $\beta \gg 1$. In the limit of large β, $P_q \approx \delta_{q,0}$ and the sum in Eq. (118) can be carried out analytically. Using Eqs. (114)–(118), we find

$$\tilde{S}(T_{21}) \sim \frac{1}{1 + \frac{4\sin^2(\omega T_{21})(\beta^4\kappa^8 + 3\beta^3\kappa^6 + 2\beta^2\kappa^4)}{(2+3\beta\kappa^2)^2}}. \tag{119}$$

The result depends only on powers of $\beta\kappa^2$, whereas the classical result (114) depends only on powers of κ. If $\kappa \geqslant 1$, $\beta \gg 1$ and $\omega T_{21} \ll 1$,

$$\tilde{S}(T_{21}) \sim \frac{1}{1 + \frac{4(\omega T_{21})^2\beta^2\kappa^4}{9}} \tag{120}$$

which is a Lorentzian having half-width $3/(2\beta\kappa^2)$.

VI. SUMMARY

We have presented a theory of coherent transients in which a sequence of optical pulses is incident on a sample of trapped atoms and gives rise to phase-matched emission from the sample. The trapping potential for the atoms is state dependent, in general, necessitating a quantum treatment of the center-of-mass motion. To carry out the calculation, we used a source-field approach, modified to account for the quantized motion of the atoms. In the simplest version of the theory, all atomic motion is frozen during the excitation pulses and during the time in which the signal is emitted. For state-independent potentials, a comparison was made with a theory in which the motion is treated classically.

Coherent transients from trapped atoms differ in a fundamental way from those for free atoms. In the case of free atoms, the Doppler phases accumulated by the various coherences in the problem are linear functions of time. As a result, it is possible to use echo techniques to effectively eliminate effects related to inhomogeneous broadening. With trapped atoms, no such methods can be used since the motional phases are not linear in time. As such, the general use of coherent transients in trapped atoms is to establish a long-lived coherence between two atomic levels that is only marginally affected by the motion in the trapping potentials. In this manner, quantum coherence can be stored in the sample and read out at a later time. Any deterioration of the signal resulting from motional effects can be calculated using the techniques developed in this paper.

Two examples were given. In the first, a long-lived coherence was established between a ground and Rydberg level for atoms trapped in a lattice potential. Phase-matched emission is produced with the use of a readout pulse. The coherence loss produced by harmonic, anharmonic, and state-dependent potentials was investigated. In the second example, a long-lived coherence was established between two, ground-state sublevels for atoms in a dipole trap, and also probed by a readout pulse. The dynamics of transit-time loss was probed in this example.

ACKNOWLEDGMENT

This work was financially supported by the ARL Center for Distributed Quantum Information, AFOSR, and the National Science Foundation.

APPENDIX

We would like to return to the non-phase-matched contribution to the signal given by Eq. (33) with $j = j'$. This term can be written as

$$S_{npm} = R_d^2\langle \mathbf{E}_-(\mathbf{R}_d,t)\cdot\mathbf{E}_+(\mathbf{R}_d,t)\rangle = N\mu_{ba}^2 R_d^2 \sum_{\mathbf{k},\mathbf{k}'}\left(\frac{\hbar\omega_{k'}}{2\epsilon_0\mathcal{V}}\right) \times\left(\frac{\hbar\omega_k}{2\epsilon_0\mathcal{V}}\right)\sin\theta_k\sin\theta_{k'}e^{i(\mathbf{k}-\mathbf{k}')\cdot\mathbf{R}_d}\boldsymbol{\epsilon}_{\mathbf{k}'}^{(1)}\cdot\boldsymbol{\epsilon}_{\mathbf{k}}^{(1)} \times\int_0^t dt'\int_0^t dt''\left\langle e^{i\mathbf{k}'\cdot\hat{\mathbf{R}}(t'')}\sigma_{ba}(t'')\sigma_{ab}(t')e^{-i\mathbf{k}\cdot\hat{\mathbf{R}}(t')}\right\rangle \times e^{i\omega_{k'}(t-t')}e^{-i\omega_k(t-t')}, \tag{A1}$$

where N is the number of atoms. We have dropped the label j since all atoms contribute equally to the signal, $\hat{\mathbf{R}}(t'')$ and $\sigma_{ba}(t'')$ and Heisenberg operators of a given atom. It is not simple to evaluate this expression in the Heisenberg representation if quantized motion must be taken into account. In fact, the best method for evaluating this term is to use a Schrödinger equation approach [29].

Going back one step in the calculation, we write

$$S_{npm} = NR_d^2\sum_{\mathbf{k},\mathbf{k}'}\left(\frac{\hbar\omega_k}{2\epsilon_0\mathcal{V}}\right)^{1/2}\left(\frac{\hbar\omega_{k'}}{2\epsilon_0\mathcal{V}}\right)^{1/2}\boldsymbol{\epsilon}_{\mathbf{k}}^{(1)}\cdot\boldsymbol{\epsilon}_{\mathbf{k}'}^{(1)}\langle a_{\mathbf{k}}^\dagger a_{\mathbf{k}'}\rangle \times e^{-i(\mathbf{k}-\mathbf{k}')\cdot\mathbf{R}_d}. \tag{A2}$$

We have anticipated the fact that only the $\lambda = 1$ polarization enters the calculation for the z-polarized excitation and readout pulses we are using. Only states that are diagonal in the atomic quantum numbers contribute to the average value of $\langle a_{\mathbf{k}}^\dagger a_{\mathbf{k}'}\rangle$; moreover, in the RWA, the only nonvanishing terms involve the ground internal states

$$\langle a_{\mathbf{k}}^\dagger a_{\mathbf{k}'}\rangle = \sum_q \rho_{aq,\mathbf{k};aq,\mathbf{k}'}(t)e^{-i\omega_{kk'}t} = \sum_q \rho^I_{aq,\mathbf{k};aq,\mathbf{k}'}(t)e^{-i\omega_{kk'}t}, \tag{A3}$$

where $\omega_{kk'} = \omega_k - \omega_{k'}$.

The Hamiltonian is

$$H = \hbar\omega_a|a\rangle\langle a| + \hbar\omega_b|b\rangle\langle b| + \sum_q[\hbar\omega_{aq}|aq\rangle\langle aq| + \hbar\omega_{bq}|bq\rangle\langle bq|] + \sum_{\mathbf{k}}[\hbar f_{\mathbf{k}}e^{i\mathbf{k}\cdot\mathbf{R}}e^{-i\omega_k t}\sigma_{ba}a_{\mathbf{k}} + \hbar f_{\mathbf{k}}^* e^{-i\mathbf{k}\cdot\mathbf{R}}e^{i\omega_k t}a_{\mathbf{k}}^\dagger\sigma_{ab}], \tag{A4}$$

where

$$f_{\mathbf{k}} = -i\mu_{ba}\left(\frac{\omega_k}{2\hbar\epsilon_0\mathcal{V}}\right)^{1/2}\sin\theta_k. \tag{A5}$$

From Schrödinger's equation, it then follows that [29]

$$\dot{\rho}^I_{aq,\mathbf{k};aq,\mathbf{k}'} = if_{\mathbf{k}'}\sum_p U_{bp;aq}(\mathbf{k}')e^{i(\omega_0-\omega_{k'})t}e^{i\omega_{bp;aq}t}\rho^I_{aq,\mathbf{k};bp,0} - if_{\mathbf{k}}^*\sum_p U^\dagger_{aq,bp}(\mathbf{k})e^{-i(\omega_0-\omega_k)t}e^{i\omega_{aq;bp}t}\rho^I_{bp,0;aq,\mathbf{k}'}, \tag{A6a}$$

$$\dot{\rho}^I_{bp,0;aq,\mathbf{k}'} = -\gamma_b\rho^I_{bp,0;aq,\mathbf{k}'} + if_{\mathbf{k}'}\sum_{p'}U_{bp',aq}(\mathbf{k}') \times e^{i(\omega_0-\omega_{k'})t}e^{i\omega_{bp';aq}t}\rho^I_{bp,0;bp',0}, \tag{A6b}$$

along with the complex conjugates of these equations. In these equations, the zero subscript stands for the vacuum state of the field, ω_0 is the b-a transition frequency, and

$$U_{bp,aq}(\mathbf{k}) = \int d\mathbf{R}[\psi_{bp}(\mathbf{R})]^* e^{i\mathbf{k}\cdot\mathbf{R}}\psi_{aq}(\mathbf{R}), \tag{A7a}$$

$$U^\dagger_{aq,bp}(\mathbf{k}) = \int d\mathbf{R}[\psi_{aq}(\mathbf{R})]^* e^{-i\mathbf{k}\cdot\mathbf{R}}\psi_{bp}(\mathbf{R}), \tag{A7b}$$

such that

$$\sum_q U_{bp,aq}(\mathbf{k})U^\dagger_{aq,bp'}(\mathbf{k}) = \sum_q U^\dagger_{bp,aq}(\mathbf{k})U_{aq,bp'}(\mathbf{k}) = \delta_{p,p'}. \tag{A8}$$

Equations (A6) are in a form that is identical to the equations in Ref. [29] and can be solved iteratively and substituted back into Eq. (A2) as in that paper. The only difference is that the matrix elements of U must be left in the form of Eqs. (A7). In this manner, we obtain [see Eqs. (22), (23a), and (25) of Ref. [29]]

$$S_{npm} = N\left(\frac{\mu_{ba}\omega_0^2\sin\theta}{4\pi\epsilon_0 c^2}\right)^2\Theta(\tau)\sum_{q,p,p'}\int d\mathbf{R}\int d\mathbf{R}'[\psi_{bp'}(\mathbf{R})]^* \times\psi_{aq}(\mathbf{R})[\psi_{aq}(\mathbf{R}')]^*\psi_{bp}(\mathbf{R}')e^{-\gamma_b(t_{\mathbf{R}'}-t_{\mathbf{R}})}e^{i\omega_0 t_{\mathbf{R}}}e^{i\omega_{bp';aq}t_{\mathbf{R}}} \times\rho^I_{bp,0;bp',0}(t_{\mathbf{R}})e^{-i\omega_0 t_{\mathbf{R}'}}e^{i\omega_{aq;bp}t_{\mathbf{R}'}} + \text{c.c.}, \tag{A9}$$

where

$$t_{\mathbf{R}} = t - t_{\text{out}} - \frac{|\mathbf{R}_d - \mathbf{R}|}{c} \approx \tau + \frac{\mathbf{R}_d\cdot\mathbf{R}}{R_d c}, \tag{A10}$$

$$t_{\mathbf{R}'} = t - t_{\text{out}} - \frac{|\mathbf{R}_d - \mathbf{R}'|}{c} \approx \tau + \frac{\mathbf{R}_d\cdot\mathbf{R}'}{R_d c}, \tag{A11}$$

$$\tau = t - t_{\text{out}} - \frac{R_d}{c}. \tag{A12}$$

When these equations are substituted into Eq. (A9) and the terms involving the dot products are retained only in the

exponential terms containing ω_0, we obtain

$$S_{npm} = 2N\left(\frac{\mu_{ba}\omega_0^2 \sin\theta}{4\pi\epsilon_0 c^2}\right)^2 \Theta(\tau) \sum_{q,p,p'} U_{bp';aq}(\mathbf{k}_d, \tau) U^{\dagger}_{aq;bp}(\mathbf{k}_d, \tau) e^{i(\omega_{bp'} - \omega_{bp})\tau} \rho^{I}_{bp,0;bp',0}(\tau), \tag{A13}$$

where

$$\mathbf{k}_d = \omega_0 \mathbf{R}_d / c \tag{A14}$$

and

$$U_{bp';aq}(\mathbf{k}_d, \tau) = \langle bp' | e^{iH_b(\mathbf{R})\tau/\hbar} e^{i\mathbf{k}_d\cdot\mathbf{R}} e^{-iH_a(\mathbf{R})\tau/\hbar} | aq \rangle, \tag{A15}$$

$$U^{\dagger}_{aq;bp}(\mathbf{k}_d, \tau) = \langle aq | e^{iH_a(\mathbf{R})\tau/\hbar} e^{-i\mathbf{k}_d\cdot\mathbf{R}} e^{-iH_b(\mathbf{R})\tau/\hbar} | bp \rangle. \tag{A16}$$

Finally, using Eq. (A8), we arrive at

$$S_{npm} = 2N\left(\frac{\mu_{ba}\omega_0^2 \sin\theta}{4\pi\epsilon_0 c^2}\right)^2 \rho_{bb}(\tau)\Theta(\tau), \tag{A17}$$

where $\rho_{bb}(\tau)$ is the total population of level b at the retarded time. Equation (A17) is a somewhat intuitive result: Since the atomic motion is constrained to distances that are much less than R_d, any *retardation* effects related to different motional states are not important and the non-phased-matched signal arises only from the total population in level b at time τ. Although this result is intuitive, we have not found a way to derive it using the Heisenberg representation.

[1] See, for example, A. Abragam, *The Principles of Nuclear Magnetism* (Oxford University Press, New York, 1961) or C. P. Slichter *Principles of Magnetic Resonance* (Harper & Row, New York, 1963).

[2] For a review, see P. R. Berman and D. G. Steel, in *Handbook of Optics*, 3rd ed., edited by M. Bass, G. Li, and E. Van Stryland (McGraw Hill, New York, 2010), Vol. IV, Chap. 11.

[3] See, for example, J. C. Bergquist, W. M. Itano, and D. J. Wineland, Phys. Rev. A **36**, 428 (1987); T. Ido and H. Katori, Phys. Rev. Lett. **91**, 053001 (2003).

[4] R. H. Dicke, Phys. Rev. **89**, 472 (1953).

[5] P. R. Berman, in *New Trends in Atomic Physics (Les Houches Session 38)*, edited by G. Grynberg and R. Stora (North Holland, Amsterdam, 1984), Vol. 1, pp. 451–514.

[6] L.-M. Duan, M. Lukin, J. I. Cirac, and P P. Zoller, Nature (London) **414**, 413 (2001).

[7] D. N. Matsukevich and A. Kuzmich, Science **306**, 663 (2004).

[8] M. Saffman, T. G. Walker, and K. Molmer, Rev. Mod. Phys. **82**, 2313 (2010).

[9] L. Li and A. Kuzmich, Nat. Commun. **7**, 13618 (2016).

[10] A. G. Radnaev, Y. O. Dudin, R. Zhao, H. H. Jen, S. D. Jenkins, A. Kuzmich, and T. A. B. Kennedy, Nat. Phys. **6**, 894 (2010).

[11] Y. O. Dudin, R. Zhao, T. A. B. Kennedy, and A. Kuzmich, Phys. Rev. A **81**, 041805 (2010).

[12] Y. O. Dudin, L. Li, and A. Kuzmich, Phys. Rev. A **87**, 031801(R) (2013).

[13] See, for example, S. Stenholm, J. Opt. Soc. Am. B **2**, 1743 (1985); Y. Castin, J. Dalibard, and C. Claude-Tannoudji, in *Light Induced Kinetic Effects of Atoms, Ions, and Molecules*, edited by L. Moi, S. Gozzini, C. Gabbanini, E. Arimondo, and F. Strumia (ETS Editrice, Pisa, 1991); G. Morigi, J. I. Cirac, K. Ellinger, and P. Zoller, Phys. Rev. A **57**, 2909 (1998).

[14] See, for example, M. Gajda, P. Krekora, and J. Mostowski, Phys. Rev. A **54**, 928 (1996); A. Orlowski, M. Gajda, P. Krekora, R. J. Glauber, and J. Mostowski, in *Quantum Communication, Computing, and Measurement 2*, edited by P. Kumar, G. M. D'Ariano, and O. Hirota (Plenums, New York, 2000), pp. 295–300.

[15] See, for example, I. A. Walmsley and L. Waxler, J. Phys. B: At. Mol. Phys. **31**, 1825 (1998), and references therein; M. Martinez-Dorantes, W. Alt, J. Gallego, S. Ghosh, L. Ratschbacher, and D. Meschede, Phys. Rev. A **97**, 023410 (2018).

[16] G. Raithel, W. D. Phillips, and S. L. Rolston, Phys. Rev. Lett. **81**, 3615 (1998).

[17] R. Zhao, Y. O. Dudin, S. D. Jenkins, C. J. Campbell, D. N. Matsukevich, T. A. B. Kennedy, and A. Kuzmich, Nat. Phys. **5**, 100 (2009).

[18] S. D. Jenkins, T. Zhang, and T. A. B. Kennedy, J. Phys. B: At., Mol. Opt. Phys. **45**, 124005 (2012).

[19] J. Lampen, H. Nguyen, L. Li, P. R. Berman, and A. Kuzmich, Phys. Rev. A **98**, 033411 (2018).

[20] See, for example, S. Wu, P. S. Striehl, and M. G. Prentiss, arXiv:0710.5479v2; their approach to calculate the transfer matrix associated with the pulsed fields is similar to ours, although it is restricted to harmonic potentials; R. H. Leonard and C. A. Sackett, Phys. Rev. A **86**, 043613 (2012); W. D. Li, T. He, and A. Smerzi, Phys. Rev. Lett. **113**, 023003 (2014).

[21] See, for example, P. R. Berman and V. S. Malinovsky, *Principles of Laser Spectroscopy and Quantum Optics* (Princeton University Press, Princeton, NJ, 2011), Secs. 19.3 and 19.4.

[22] P. R. Berman and V. S. Malinovsky, *Principles of Laser Spectroscopy and Quantum Optics* (Princeton University Press, Princeton, NJ, 2011), Sec 10.1.

[23] P. R. Berman and V. S. Malinovsky, *Principles of Laser Spectroscopy and Quantum Optics* (Princeton University Press, Princeton, NJ, 2011), Chap. 9.

[24] T. Topcu and A. Derevianko, Phys. Rev. A **88**, 043407 (2013).
[25] P. R. Berman, Am. J. Phys. **81**, 190 (2013).
[26] See, for example, S. M. Barnett and P. M. Radmore, *Methods in Theoretical Quantum Optics* (Oxford University Press, Oxford, 1997), Sec. 4.4.
[27] See, for example, T. R. Carver, Am. J. Phys. **39**, 1225 (1971); K. Ochs, Eur. J. Phys. **32**, 479 (2011).
[28] J. L. Cohen and P. R. Berman, Phys. Rev. A **54**, 5262 (1996).
[29] P. R. Berman, Phys. Rev. A **69**, 022101 (2004).